



Halogen activation in the plume of Masaya volcano: field observations and box model investigations

Julian Rüdiger^{1,2}, Alexandra Gutmann¹, Nicole Bobrowski^{3,4}, Marcello Liotta⁵, J. Maarten de Moor⁶, Rolf Sander⁴, Florian Dinger^{3,4}, Jan-Lukas Tirpitz³, Martha Ibarra⁷, Armando Saballos⁷, María Martínez⁶,
5 Elvis Mendoza⁷, Arnoldo Ferrufino⁷, John Stix⁸, Juan Valdés⁹, Jonathan M. Castro¹⁰, and Thorsten Hoffmann¹

¹Institute of Inorganic and Analytical Chemistry, Johannes Gutenberg-University, Mainz, Germany

²Chair of Environmental Chemistry and Air Research, Technical University Berlin, Berlin, Germany

³Institute for Environmental Physics, University of Heidelberg, Heidelberg, Germany

10 ⁴Max-Planck Institute for Chemistry, Mainz, Germany

⁵Istituto Nazionale di Geofisica e Vulcanologia, Sezione di Palermo, Italy

⁶Observatorio Vulcanológico y Sismológico de Costa Rica Universidad Nacional, Heredia, Costa Rica

⁷Instituto Nicaragüense de Estudios Territoriales, Nicaragua

⁸Department of Earth and Planetary Sciences, McGill University, Montreal, Canada

15 ⁹Laboratorio de Química de la Atmósfera, Universidad Nacional, Heredia, Costa Rica

¹⁰Institute of Geosciences, Johannes Gutenberg University Mainz, Mainz, Germany

Correspondence to: Thorsten Hoffmann (t.hoffmann@uni-mainz.de)

20

Abstract. Volcanic emissions are a source of halogens to the atmosphere. Rapid reactions convert the initially emitted hydrogen halides (HCl, HBr, HI) into reactive species e.g. BrO, Br₂, BrCl, ClO, OCIO and IO. The activation reaction mechanisms in the plume consume ozone (O₃), which is entrained by in-mixed ambient air. In this study, we present observations of the oxidation of bromine, chlorine and iodine during the first 11 minutes after emission, investigating the
25 plume of Santiago Crater of Masaya volcano in Nicaragua. Two field campaigns were conducted, in July 2016 and September 2016. The sum of the reactive species of the respective halogens were determined by gas diffusion denuder sampling followed by GC-MS analysis, while the total amounts of halogens and sulfur amounts were obtained by alkaline trap sampling with subsequent IC and ICP-MS measurements. Both ground and airborne sampling with an unmanned aerial vehicle (including a denuder sampler in combination with an electrochemical SO₂ sensor) was performed at different distances from the crater rim.
30 The in-situ measurements were accompanied by remote sensing observations (DOAS). For bromine, the reactive fraction increased from 0.20 ± 0.13 at the crater rim to 0.76 ± 0.26 at 2.8 km downwind, while chlorine showed an increase of the reactive fraction from $(2.7 \pm 0.7) \times 10^{-4}$ to $(11 \pm 3) \times 10^{-4}$ in the first 750 m. Additionally, a reactive iodine fraction of 0.3 at the crater rim and 0.9 at 2.8 km was measured. No significant increase in BrO/SO₂ molar ratios was observed with the estimated age of the observed plume ranging from 1.4 min to 11.1 min. This study presents a comprehensive gas diffusion denuder data
35 set on reactive halogen species and compares BrO/SO₂ ratios with the sum of all reactive Br species. With the observed field data, a chemistry box model (CAABA/MECCA) enabled the reproduction of the observed progression of the reactive bromine



to total bromine ratio. An observed contribution of BrO to the reactive bromine fraction of about 10 % was reproduced in the first minutes of the model run. The model results emphasize the importance of ozone entrainment into the plume for the reproduction of the measured reactive bromine formation and the dependence on the availability of H_xO_y and NO_x .



1. Introduction

Volcanoes are known to be important emitters of atmospheric trace gases and aerosols, both through explosive eruptions and persistent quiescent degassing (von Glasow et al., 2009). The most abundant gases in volcanic emissions are water, carbon dioxide, sulfur compounds and hydrogen halides (Symonds et al., 1994). Typically, halogen emissions are largely dominated by chlorine (HCl) and fluorine (HF), while bromine (HBr) and iodine (HI) are three and five orders of magnitude less abundant than chlorine and fluorine, respectively (e.g., Aiuppa et al., 2005; Pyle and Mather, 2009). Despite their low abundance, the heavy halogens (bromine and iodine) can have significant impact on the chemistry of the atmosphere (e.g., von Glasow, 2010; Saiz-Lopez and von Glasow, 2012; Platt and Bobrowski, 2015). The chemical composition of volcanic plumes is the subject of a large number of studies, usually aimed at gaining insights into subsurface processes, such as the degassing of magma in connection with changes in volcanic activity. In addition, the effects of volcanic gases on the atmosphere and biosphere at local, regional and global scales are also of interest, e.g., acid deposition (wet and dry), nutrient input, aerosol formation and effects on the solar radiation balance.

Volcanic halogen emissions have been studied for years (e.g., Noguchi and Kamiya, 1963; Giggenbach, 1975) and the determination of chlorine and sulfur is a common procedure in such gas geochemical investigations. Bromine only attracted more attention in later years, when in various studies the reactive bromine species BrO was observed in volcanic plumes (e.g., Bobrowski et al., 2003; Oppenheimer et al., 2006). This proved that not only sulfur species (H_2S , SO_2) undergo oxidation by ambient reactants (such as OH, O_3), and laid the basis for various studies on oxidized halogen species (BrO, ClO, OCIO, IO). Despite the low abundance of bromine in volcanic gas emissions, the relatively simple detection of BrO by differential optical absorption spectroscopy (DOAS) promoted research on the origin and fate of BrO in volcanic plumes. Based on thermodynamic modelling, Gerlach (2004) hypothesized that BrO is not primarily emitted by volcanoes, but is formed only after the initial emissions are mixed with entrained ambient air. Since SO_2 can also be easily measured by DOAS, the ratio of BrO to SO_2 is used as a dilution-compensated observation parameter, since over an observation period of minutes to hours is assumed that the oxidation of SO_2 plays a minor role (McGonigle et al., 2004).

An increase in the BrO/ SO_2 ratio with increasing distance from the emitting vent was observed at various volcanoes (e.g., Bobrowski et al., 2007; Vogel, 2012; Gliß et al., 2015), together with variations of BrO/ SO_2 in a lateral plume dimension with higher ratios at the edges of the plume (e.g., Bobrowski et al., 2007; Louban et al., 2009; General et al., 2015; Kern and Lyons, 2018). This was explained by a limited transfer of atmospheric O_3 to the center of the plume, which is thought to promote the formation of BrO in a chain reaction mechanism involving heterogeneous chemistry. Shortly after the discovery of the reactive bromine species BrO, reactive chlorine species, ClO and OCIO, were also observed using the same DOAS techniques (e.g., Lee et al., 2005; Bobrowski et al., 2007; Donovan et al., 2014; Theys et al., 2014; General et al., 2015; Gliß et al., 2015; Kern and Lyons, 2018). It was found that the abundance of ClO and OCIO is on the same order of magnitude as BrO, in contrast to total chlorine, which is typically three orders of magnitude more abundant than bromine. The formation of reactive chlorine species is considered to be a secondary product of the activation cycle of bromine (see Table 1). Recently, reactive iodine



species have also been detected by satellite observations in the plume of Kasatochi (Schönhardt et al., 2017), but could not be confirmed by ground-based measurements so far.

Both the transformation of halogen species in the plume and their fate in the atmosphere are of interest. In particular, the clarification of the question of the amounts emitted into the atmosphere and the distribution of the halogens emitted by quiescent (i.e., passive, non-eruptive) and eruptive degassing are of interest. The global SO₂ flux has been estimated as 23 Tg/yr for the period from 2004-2016 (Carn et al., 2017), resulting in estimated halogen fluxes of the same order for chlorine and three orders of magnitude lower for bromine, taking into account global mean sulfur/halogen ratios (Aiuppa et al., 2009). Bromine from various sources (e.g. polar regions, salt lakes, volcanoes) is involved in tropospheric and stratospheric ozone depletion (e.g., Wennberg, 1999; Rose et al., 2006; Simpson et al., 2007). Tropospheric ozone depletion has also been observed in volcanic plumes (e.g., Hobbs et al., 1982; Kelly et al., 2013; Surl et al., 2015), which supports the proposed reaction mechanisms for BrO formation via autocatalytic chain reactions. Recent observations of halogen oxides by satellites (e.g., Theys et al., 2009; Carn et al., 2016) and aircraft missions (Millard et al., 2006) confirm the injection of volcanic halogens into the stratosphere by large eruptions and therefore their potential impact on stratospheric ozone. In addition to effects of volcanic degassing on atmospheric chemistry, measurements of volcanic emission have become an important and well-established tool in the assessment of volcanic hazard, and gas monitoring is used at many volcanoes around the world (e.g., Carroll and Holloway, 1994; Aiuppa et al., 2007; de Moor et al., 2016).

It has been also observed that the BrO/SO₂ gas ratio changes with the activity of volcanoes. Bobrowski and Giuffrida (2012) observed lower BrO/SO₂ ratios in Etna's plume during eruptive phases. Also long-term observations using DOAS by Lübcke et al. (2014), who used stationary spectrometers within the NOVAC network (Galle et al., 2010), showed a decrease in the BrO/SO₂ ratio before explosive activity at Nevado del Ruiz volcano. More recently, a study by Dinger et al. (2018) at the Cotopaxi volcano (Ecuador) showed low BrO/SO₂ ratios at the beginning of eruptive activity compared to data at declining activity. Finally, Warnach et al. (2019) found low BrO/SO₂ ratio during high explosive periods and an increased BrO/SO₂ ratio during low explosive periods at Tungurahua volcano.

However, the use of the BrO/SO₂ ratio as a precursor activity signal is still being discussed, although it is automatically obtained by remote sensing instruments. That is due to the fact that BrO is a reactive secondary gas species and its formation potentially depends on atmospheric variables such as humidity, oxidant abundance, solar radiation, and aerosol surface. The BrO/SO₂ ratio might not always or only partially be controlled by the total bromine emission at a particular volcano under study (Roberts et al., 2018). Further knowledge of the chemistry that drives halogen activation is therefore required.

This article presents a comprehensive data set obtained during three field campaigns at Masaya volcano using several measurement techniques, including DOAS (e.g. Bobrowski et al., 2003), MultiGAS (Shinohara, 2005; Aiuppa et al., 2006), alkaline trap (e.g., Wittmer et al., 2014) and gas diffusion denuder sampling (e.g., Rüdiger et al., 2017). The use of an unmanned aerial vehicle (UAV) (e.g., Rüdiger et al., 2018; Stix et al., 2018) enabled the sampling of a downwind plume for the



investigation of halogen-induced plume aging processes, which is realized by atmospheric modelling of plume halogen chemistry.

2. Volcanic plume halogen chemistry

5

Besides numerous field surveys at various volcanoes, several atmospheric modelling studies have been conducted, which have improved our understanding of the complex chemical reactions in volcanic plumes marking the interface between volcanic trace gases (and aerosols) and ambient air. Two models were developed to simulate the in-plume chemistry, MISTRA (Bobrowski et al., 2007; von Glasow, 2010) and PlumeChem (Roberts et al., 2009; Roberts et al., 2014), respectively. While MISTRA is a one-dimensional box model including multiphase chemistry, PlumeChem additionally includes plume dispersion and 3D simulation by employing a multiple grid box mode, but only rudimentary multiphase chemistry. More recently, regional model features have been incorporated (Jourdain et al., 2016). Both models are initialized with the gas composition of a so-called “effective source region”, which encompasses the compositional results of a thermodynamic equilibrium model (e.g., Gerlach, 2004; Martin et al., 2006). Different mixtures of magmatic gas and ambient air yield the hot gas mixture of the “effective source region”, which is quenched to ambient temperature and then mixed with ambient air including O₃, OH and NO_x. The sensitivity of the model was evaluated by characterizing the impact of variations of input parameters, such as the halogen flux, volcanic aerosol load, plume-air mixing and oxidant entrainment (Roberts et al., 2014) on reactive Br species formation and ozone depletion event reproduction (e.g., Roberts, 2018; Kelly et al., 2013; Surl et al., 2015).

The initially emitted HBr is converted into reactive species via an autocatalytic mechanism, involving multiphase reactions, which constitute so-called “bromine explosion” (von Glasow et al., 2009). Under ozone consumption, Br radicals – formed by high temperature dissociation in the “effective source region” – react to BrO (Table1, R1), which in turn reacts with HO₂ or NO₂ to form HOBr (R2) or BrNO₃, respectively. A subsequent uptake into aerosol enables the conversion of HBr into Br₂, which partitions into the gas phase and is photolyzed to give two Br radicals and start the cycle again (R5a). The self-reaction of two BrO to give Br₂ and O₂ is suggested to be the major ozone-depleting channel at high bromine concentrations as in a young plume (Roberts, 2018). Once HBr becomes depleted, the uptake of HOBr/BrNO₃ may promote the formation of BrCl, which also consumes O₃ and forms reactive chlorine species such as ClO and OClO (R6, R8). The major reaction pathways that involve the formation and degradation of BrO in volcanic plumes are shown in Table1.

An extensive review of the advances of bromine speciation in volcanic plumes including a comparison of different model approaches has recently been presented by Gutmann et al (2018). In this study, we present in situ measurements along with remote sensing data on the activation of Br, Cl and I in the volcanic plume of Masaya and further investigate the involved halogen species by atmospheric model simulations. Although fluorine has been measured as well, it is not discussed in detail in this study, due to the high water solubility and the non-reactivity of fluoride towards oxidation.



Table 1: Overview on halogen reactions in volcanic plumes (X = Cl, Br)

$\text{Br} + \text{O}_3 \rightarrow \text{BrO} + \text{O}_2$	(R1)
$\text{BrO} + \text{HO}_2 \rightarrow \text{HOBr}_{(\text{g})} + \text{O}_2$	(R2)
$\text{HBr}_{(\text{g})} \rightarrow \text{Br}^-_{(\text{aq})} + \text{H}^+_{(\text{aq})}$	(R3)
$\text{HOBr}_{(\text{aq})} + \text{Br}^-_{(\text{aq})} + \text{H}^+_{(\text{aq})} \rightarrow \text{Br}_{2(\text{g})} + \text{H}_2\text{O}_{(\text{aq})}$	(R4a)
$\text{HOBr}_{(\text{aq})} + \text{HCl}_{(\text{aq})} \rightarrow \text{BrCl}_{(\text{g})} + \text{H}_2\text{O}_{(\text{aq})}$	(R4b)
$\text{Br}_{2(\text{g})} \xrightarrow{h\nu} 2 \text{Br}$	(R5a)
$\text{BrCl}_{(\text{g})} \xrightarrow{h\nu} \text{Br} + \text{Cl}$	(R5b)
$\text{Cl} + \text{O}_3 \rightarrow \text{ClO}$	(R6)
$\text{BrO} + \text{BrO} \rightarrow \text{Br}_2 + \text{O}_2$	(R7)
$\text{BrO} + \text{ClO} \rightarrow \text{OClO} + \text{Br}$	(R8)

3. Measurements

3.1. Site description and flight/sample strategy

Masaya volcano in Nicaragua is a shield volcano with a caldera size of 6 km x 11 km. The caldera hosts a set of vents, of which the Santiago pit crater, that formed in 1858-1859, is currently active (McBirney, 1956). Since mid-November 2015, Santiago crater has contained a persistent more superficial lava lake (~40 m x 40 m). The increment of the general lava lake level inside the Santiago pit crater has been accompanied by increased emissions of volcanic gases, making it one of the largest contributors in SO₂ emissions of the Central American volcanic arc (Martin et al., 2010; de Moor et al., 2017; Aiuppa et al., 2018). Due to high emission rates and the low-altitude ground-hugging plume, Masaya volcano has a severe environmental impact on the downwind areas, affecting human and animal health and vegetation (Delmelle et al., 2002). With its easy accessibility by car and low altitude, the emissions of Masaya volcano have been studied extensively throughout the last decades. Of particular note is the establishment of halogen-to-sulfur ratios, determined to be in the order of 0.3-0.7 for chlorine and 3×10^{-4} for bromine (e.g., Witt et al., 2008; Martin et al., 2010; de Moor et al., 2013). These halogen values are considered to be on the high end observed in magmas and plumes, yet are rather typical for arc volcanism (Aiuppa, 2009; Gutmann et al., 2018). Reactive bromine species (BrO) measurements were reported in the past (Bobrowski and Platt, 2007; Kern et al., 2009). Continuous composition monitoring (by Multi-GAS) is realized (since 2014) and gas data for the onset of the superficial lava lake was presented by Aiuppa et al. (2018).

In our field campaigns in 2016, UAV-based and ground-based sampling approaches were undertaken to study the plume of Masaya volcano with a focus on halogen emissions and atmospheric reactions of the emitted halogens. Samples were taken on the ground level at the edge of Santiago crater (Figure 1) at two locations (lookout south and pole site), at the top of the rim of Nindirí crater (Nindirí rim) and at the Cerro Ventarrón. UAV-based sampling was conducted in the plume hovering over the Nindirí crater and above the caldera bottom and caldera rim (red points in Figure 1 (d)). The plume was sampled over a distance of about 2.8 km, covering an estimated age of 10 minutes, depending on the wind velocity.

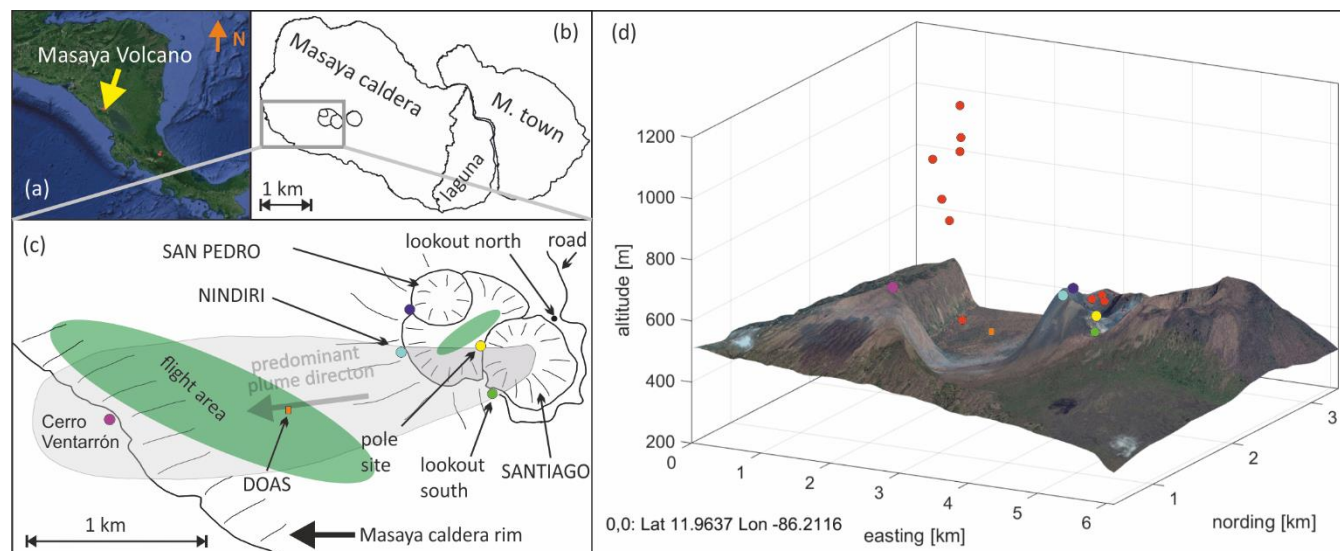


Figure 1: (a) location of Masaya volcano in Central America (© Google); (b) Masaya pit crater system in the Masaya caldera; (c) and (d) flight area (green patch and red points) and sampling locations marked by colored circles in sketched map and 3D plot.

5 3.2. Alkaline traps

Total halogen amounts were obtained by ground based sampling, using alkaline traps (Raschig tube (RT) and Drechsel bottle (DB)) (Liotta et al., 2012; Wittmer et al., 2014) at the locations marked in Figure 1. The alkaline solution quantitatively captures acidic gas species, due to an acid-base reaction, and enables the determination of total halogens (F, Cl, Br, I) and sulfur (S) concentrations. The sampled solutions were measured by ion chromatography (IC) and inductively coupled plasma mass spectrometry (ICP-MS) at the Geochemistry Laboratories of the Istituto Nazionale di Geofisica e Vulcanologia, Palermo (Italy). A 1 M NaOH solution was used applying the RT and a 4 M NaOH solution when using the DB. Both solutions were made from NaOH 99 % purity, Merck, Germany, in 18.2 MΩ cm⁻¹ water. The plume samples were pumped through the RT by using a GilAir Plus pump (Sensidyne, USA) for about one hour at 2.8 to 4 Lmin⁻¹. Total volume data logging enabled mixing ratio calculation of the RT samples. With the Drechsel bottle a custom-built pump –without data logging - was used at a flow rate of approx. 1 L min⁻¹ for 18 to 30 hours. These samples were used for gas ratio comparisons over a longer time period.

3.3. Gas diffusion denuder sampling

Reactive halogen species RHS were sampled by gas diffusion denuder samplers using 1,3,5-trimethoxybenzene as a reactive coating (Rüdiger et al., 2017) on borosilicate brown-glass tubes with a diameter of 0.9 cm. An electrophilic substitution



reaction occurs within this coating, effectively trapping halogen species with an oxidation state (OS) of +1 or 0 (HalX, e.g., Br₂ or BrCl), which are considered as reactive species in contrast to the -1 OS species Br_(aq) or HBr_(g). Ground-based denuder measurements employed a serial setup of two denuders (2 x 50 cm) at a flow rate of 250 ml min⁻¹ using a GilAir Plus pump and were conducted simultaneously to the RT sampling for 60 minutes to give the ratios of reactive species to total halogens (e.g., HalX/Br) or total sulfur (e.g., HalX/S). For the UAV based sampling, a remotely controlled sampler (called Black Box) was used, described in detail in Rüdiger et al. (2018). The typical sampling flow rate was about 180 ml min⁻¹ for 5 to 15 minutes. The Black Box enabled logging of the sampling duration and SO₂ mixing ratios via the built-in SO₂ electrochemical sensor. Furthermore, the SO₂ sensor signal was transmitted to the remote control, which helped to identify regions of high SO₂ concentrations in real-time and therefore enabling location of dense plume areas. The SO₂ signal of the sensor was time integrated over the sampling period of the denuders to derive the HalX/S ratios at the location where the UAV hovered during sampling.

3.4. Unmanned aerial vehicle sampler

The UAV used for this study is a small four-rotor multicopter with foldable arms (Black Snapper, Globe Flight, Germany) called RAVEN (Rüdiger et al., 2018). We achieved flight times of up to 15 minutes with a payload of approximately 1 kg, depending on the sampling setup. GPS data of the flights was recorded onboard by using the micro-SD data logger (Core 2, Flytrex, Aviation, Tel Aviv, Israel) with a 2 Hz time resolution. The four batteries of the UAV were charged in the field with a car battery, enabling up to eight flights per day.

3.5. DOAS

DOAS measurements of SO₂ and BrO were performed by a scanning-DOAS station from the NOVAC network (Galle et al., 2010), which is located approximately 1.5 km WSW of Santiago crater at an altitude of 387 m a.s.l. (Aiuppa et al., 2018). This UV-spectrometer records the intensity spectra of the diffuse solar radiation over a wavelength range from 280-450 nm for different viewing angles by scanning the sky from horizon to horizon at steps of 3.6°. For most of the time, the volcanic plume transacts the scan plane nearly orthogonally. The slant column densities are retrieved from these spectra via the DOAS method (Platt and Stutz, 2008). Due to the rather high BrO detection limit, spectral and arithmetical averaging is required for a reliable retrieval of the BrO SCDs and ultimately the calculated BrO/SO₂ molar ratios. As a drawback, the temporal resolution of the BrO and BrO/SO₂ data is reduced to a data point roughly every 30 min. For a detailed methodological description see Lübcke et al. (2014) and Dinger (2019). Due to a data gap caused by an instrument outage, DOAS data for July 2016 was not available and therefore the times series only covers the later part of the field study. The obtained BrO/SO₂ ratios were investigated for a period between 06th of August 2016 and 30th of September 2016. The plume age was estimated by employing wind speed data obtained at the airport of Managua (Iowa State University, 2018), 18 km to the north of Masaya volcano. An estimated plume height of 600 to 1000 m a.s.l. resulted in an average plume distance to the vent above the DOAS instrument of 1.7 km, considering a direct path of travel from the vent to the zenith position above the instrument. This distance was divided by the



wind speed which gave BrO/SO₂ ratios for a plume age between 1.4 and 11.1 minutes (see supplementary material Figure S1), which is reasonable compared to the estimated plume age for the UAV- and ground based data. There, an average plume age for the 2.8 km distance to the vent was estimated to be 9.3 minutes using a mean wind speed of 5 m/s. This is an average wind speed that was estimated by ground based wind speed measurements with a handheld anemometer during the field campaign.

5

4. Modelling

In order to compare the results of the field measurements of RHS with theoretical predictions, the box model CAABA/MECCA (Sander et al., 2011) was used. In its base configuration, CAABA/MECCA simulates the chemistry of an atmospheric air parcel. In this study, however, it was adapted to the conditions of a volcanic plume. The atmospheric box model was initialized with the gas composition of the “effective source region” that was calculated by the thermodynamic equilibrium model HSC (HSC Roine A (2007) HSC chemistry 6.1. Tech. rep. Outotec Research Oy) and then quenched with ambient air to start the atmospheric model similar to earlier works (e.g., Gerlach, 2004; Bobrowski et al., 2007; Roberts et al., 2009; Roberts et al., 2014).

4.1. Thermodynamic equilibrium model (HSC)

Data from field measurements in 2016, while the lava lake was visually present with an extent of about 40 m in diameter, determined the initial conditions for the model runs. SO₂, CO₂ and H₂O mixing ratios were derived from Multi-GAS measurements (de Moor et al. 2017; Rüdiger et al. 2018; Stix et al. 2018) and halogen amounts from the alkaline trap sampling. The sum of all gas mixing ratios were set to 100 percent to estimate the magmatic gas composition. H₂S and H₂ were not detectable (H₂S/SO₂ ratio < 0.01) by the Multi-GAS measurements and therefore neglected in the magmatic gas contribution. The high temperature magmatic gas composition was mixed with different percentages of ambient atmospheric background air resulting in different atmospheric-magmatic gas ratios (V_A:V_M), according to the calculations of Martin et al. (2006). The atmospheric background gas composition was taken from Roberts et al. (2014) (who used atmospheric background data for Etna volcano, Italy), since no detailed data on the atmospheric background composition at Masaya volcano was available, regarding trace gas species. The HSC model was reduced to produce gas species containing the elements (C, S, O, N, H, F, Cl, Br and I) and the temperature in the HSC model was arbitrarily set to 1000 °C. Similar to Roberts et al. (2009), this magmatic/ambient gas mixture of the “effective source region” was quenched with ambient air in order to obtain different mixing ratios of all gas species (SO₂ mixing ratios are used as a proxy) for the initialization of the CAABA/MECCA model (Figure 2).

A list of the input and output species for the thermodynamic modelling of the high-temperature “effective source region” using the HSC model can be found in the supplementary material, as well as the atmospheric background composition (Table S 1).

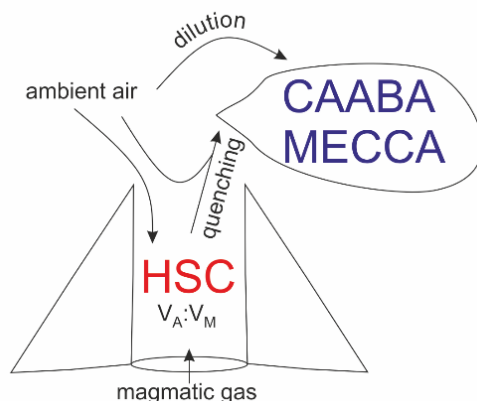


Figure 2: Sketch of the initialization process of the model.

4.2. Atmospheric box model (CAABA/MECCA)

The start point of the atmospheric chemistry box model was set to be within Santiago Crater, so the plume reaching the crater rim has already experienced chemical reactions. Thus, we were able to compare our field measurement results with the model output.

Throughout the box model run, further dilution with the same ambient air mixture was employed to entrain oxidants into the plume. In the box model, the dilution was achieved by adding an amount of ambient air, mixing it and then removing the same amount of mixed plume at a rate that achieves dilution to $1/e$ (0.37) over the dilution times listed in Table 2. Aerosol data was taken from optical particle counter measurements (Stix et al., 2018), which showed bimodal distribution of particles with diameters of 1.1 and 2.4 μm and $\text{PM}_{2.5}$ values reaching up to $5.4 \times 10^3 \mu\text{g m}^{-3}$. However, in CAABA/MECCA only a unimodal aerosol distribution was employed. The aerosol particle number concentrations and particle radii were varied in the model runs (see Table 2) to cover various particles masses and surfaces, including those observed in the field measurements. The aerosol chemical composition was set to be an 1:1 sulfuric acid / sulfate aerosol with ion concentrations according to the Köhler equation (Laaksonen et al., 1998) with given radii, temperature and relative humidity. Other parameters used in the CAABA/MECCA box model were a temperature of 298 K, a relative humidity of 80 % and a pressure of 960 hPa. The solar radiation was chosen for the 1st of August at 12:00 with the solar zenith angle at the Masaya latitude of 11.98 °N. For this, the photolysis module JVAL was used (Sander et al., 2014). The runtime of the model was 25 minutes with a time step of 2 seconds to capture the estimated plume age of the field samples. With the initialization of the model, particulate sulfur accounts for less than 1 % of the total sulfur content. Comparison of the measurement data with the box model data was conducted by identifying model scenarios, which produce formation and progression of the bromine species and their ratios to total bromine and sulfur amounts comparable to what was measured. For this, the progression of the respective reactive bromine to total bromine ratios were fitted by applying an exponential function given by equation (1), with c being the average ratio measured (or modelled) at a distance of about 2.8 km:



$$f(x) = a * \exp(-b * x) + c \quad (\text{Eq. 1})$$

Two approaches were investigated by comparing molecular reactive bromine species BrX (Br₂, BrCl, BrNO₂, BrNO₃, HOBr, BrO) and all reactive bromine species (r-Br), which also includes Br radicals (r-Br = BrX + Br radicals, see Table 2). The progressions of the respective halogen species (BrX and r-Br) were fitted over the estimated plume age and the fit coefficients were compared with the coefficients from the field data to find the best agreement by minimizing the deviation of the respective fit parameters.

Table 2: Overview on chemical species abbreviations

BrX	Br ₂ , BrCl, BrNO ₂ , BrNO ₃ , HOBr, BrO
r-Br	BrX + Br radicals
Br	all Br species (measured by alkaline trap)
ClX	Cl ₂ , ClNO ₂ , ClNO ₃ , HOCl, ClO, OClO
r-Cl	ClX + Cl radicals
Cl	all Cl species (measured by alkaline trap)
IX	I ₂ , IO, IONO ₂ , IONO ₃ , HOI, OIO, HIO ₃ , ICl, IBr
r-I	IX + I radicals
I	all I species (measured by alkaline trap)
NO _x	NO, NO ₂
H _x O _y	OH, H ₂ O ₂ , HO ₂



Table 3: Thermodynamic (HSC) and box (CAABA/MECCA) model parameters, in bold measured parameters at the Santiago crater rim.

#	Parameter	Values		
1	HSC magmatic gas composition	Species	X/SO ₂ (mol/mol)	Mixing ratio in the magmatic gas
		SO ₂	1.0	0.015
		H ₂ O	62.3	0.93
		CO ₂	2.94	0.044
		HF	0.07	1.05×10 ⁻³
		HCl	0.69	1.03×10 ⁻²
		HBr	7.4×10 ⁻⁴	1.1×10 ⁻⁵
		HI	4.7×10 ⁻⁵	6.93×10 ⁻⁷
2	HSC V _A :V _M	0:100, 2:98, 5:95, 10:90, 15:85, 35:65, 50:50		
3	Quenched SO ₂ mixing ratios at model start	1000 ppmv, 500 ppmv, 300 ppmv, 30 ppmv, 6 ppmv		
4	Reactive H _X O _Y , NO _X (NO, NO ₂) species	HSC output (mag) or atmospheric background (air) (see Table S1)		
5	Dilution time to 1/e	10, 30, 60 minutes		
6	Aerosol number concentration	1×10 ⁸ m ⁻³ , 1×10 ⁹ m ⁻³ , 3×10 ⁹ m ⁻³ , 5×10 ⁹ m ⁻³		
7	Aerosol particle size	50, 300, 900, 1500 nm		
8	Aerosol volume	5×10 ⁻¹⁴ to 9×10 ⁻⁸ m ³ /m ³		
9	Aerosol surface	3×10 ⁻⁶ to 0.16 m ² /m ³ (1.5 ×10⁻² m²/m³)		

5. Results and discussion

For samples taken on the ground e.g., at the crater rim of Santiago or on the rim of Nindiri the data includes denuder and RT samples, while for aerial samples (e.g., caldera valley) RT data are not available. Ratios of the reactive halogens to sulfur or total halogen amounts were derived by employing the RT data and in the case of aerial samples data from the SO₂ electrochemical sensor. A comparison of a RT sample simultaneously taken to Multi-GAS measurements resulted in 4.18 ± 0.22 ppm of SO₂ in the RT sample and an average mixing ratio of 3.95 ± 0.20 ppm SO₂ for the Multi-GAS data. Based on Multi-GAS measurements conducted during the field campaign, which showed no presence of H₂S, it is assumed that the sulfur content of the alkaline trap samples originates from SO₂. Therefore, we regard the alkaline trap sulfur and the electrochemical sensed SO₂ as equivalent and use measured SO₂ mixing ratios as a plume dilution marker, which is in accordance with SO₂ reactivity observations of McGonigle et al. (2004) at Masaya volcano. The uncertainties of the obtained ratios are derived by the propagation of the errors of the analytical procedure and the sampling parameters. This includes the errors of GC-MS, IC and ICP-MS measurements as well as uncertainties in the sampling flow rate and the solution volume.



5.1. Total halogens

Sampling activities for a period of 9 days in July 2016 and 5 days in September 2016 gave 36 sample sets consisting of different combinations of alkaline traps, denuder and SO₂ sensor data (see Table S2). The alkaline trap samples were analyzed by IC and ICP-MS, whereas sulfur, fluorine and chlorine amounts were obtained by IC, bromine and iodine amounts were derived from ICP-MS analysis. The average molar (mol/mol) halogen to sulfur ratios (Hal/S) from samples taken at the crater rim are 0.07 ± 0.03 for fluorine, 0.69 ± 0.08 for chlorine, $7.4 \times 10^{-4} \pm 1.7 \times 10^{-4}$ for bromine and $4.6 \times 10^{-5} \pm 1.0 \times 10^{-5}$ for iodine respectively (see Table 4).

The halogen to sulfur ratios (Hal/S) obtained during the field campaign were categorized into groups with respect to their different sampling location, date and method (see Figure 3). For fluorine, bromine and iodine the deviation within the 4M NaOH solution samples (Drechsel samples) is larger than with chlorine. Whereas chlorine shows only a 6% deviation, deviations of 29% for I, 43% for Br and 62% for F are determined for the samples taken with DB. The 4M solutions were typically left at the site for overnight sampling (18–24 h). During this time, precipitation events might have affected the incorporated plume Hal/S ratios by different scavenging efficiencies for each halogen compound and water-solubilities of the respective gases. Duffel et al. (2003) also reported a high variability in HF data (obtained by Open-path Fourier transform infrared spectroscopy) and associated it to scavenging of the soluble HF by a condensed plume during overnight measurements. Different deposition rates of particulate and gas phases could cause loss of particles prior to sampling and therefore a larger variability in Hal/S ratios in overnight samples. Regarding the sampling location, on a first glance a difference in the Hal/S ratio can be noted between the crater rim and Nindirí rim. However, excluding samples that were taken under rather diluted plume conditions with a mean sulfur mixing ratio of < 1 ppmv, the difference in the Hal/S ratio between crater rim and Nindirí rim becomes negligible. While halogen and sulfur amounts in the considered samples were above the detection limit, one potential reason for discrepancies in the ratios may derive from contamination by entrained ash in the RT, although attention had been taken by pointing the RT-entrance away from the source. With lower overall plume enrichment in certain samples halogen-laden particle uptake could be a source for an increased Hal/S ratio with the Nindirí rim samples. A significant change in the I/S ratio between July and September is observable, which showed higher values in September, while the other Hal/S ratios do not change largely over this period (see supplementary material Figure S5). Using an average flux of 3029 ± 1396 t/day (1σ) of SO₂, obtained by car DOAS traverses during the field work in July 2016 (de Moor et al. 2017) the following halogen fluxes were calculated for July 2016: 66 ± 40 t/day of HF, 1190 ± 130 t/day of HCl, 2.8 ± 0.7 t/day of HBr and 0.28 ± 0.06 t/day of HI. The cumulative error of the halogen fluxes is derived from the propagation of the SO₂ flux and the halogen to sulfur ratio uncertainties. The data set for halogens obtained in this study complements the measurements (filter packs) by Witt et al. (2008) in 2006 and Martin et al. (2010) in 2009 and is the first detailed data set on halogens for Masaya since the superficial appearance of the lava lake (see Table 5). The Cl/S ratio is within the uncertainty of that reported by Martin et al. (2010) and twice as high as Witt et al. (2008). While in 2016 the F/S ratio was about half of what was measured in 2009, the abundances of the heavier halogens have increased by a factor of ~2 for Br and ~3 for I compared to 2009, and are therefore



significantly higher than the ratios in 2006 and 2009. Based on the CO_2/SO_2 ratio, Aiuppa et al. (2018) reported increased CO_2 emissions alongside the increased level and extension of the superficial lava lake. For the period prior to the appearance of the lava lake the CO_2/SO_2 ratios were already higher than the reported ones for 2006 and 2009 and as well as the ones determined for the end of July 2016 until March 2017. Aiuppa et al. (2018) presented an average CO_2/SO_2 ratio of 5.5 ± 1.9 during the period of our measurements compared to 3.4 ± 0.5 in 2006 (Witt et al. 2008) and 2.7 ± 0.3 in 2009 (Martin et al. 2010) or 2.3–2.5 in 1998 (Burton et al., 2000). Alongside the halogen measurements in this study also CO_2/SO_2 ratios were obtained in July 2016 (de Moor et al., 2017; Rüdiger et al., 2018) that represent rather short snapshot periods of few hours and resulted in values of 4.0 ± 0.6 and 3.6 ± 0.6 , respectively, so only slightly lower than the average of Aiuppa et al., 2018. Compared to 2006 and 2009 the increased Br/S and I/S ratios in 2016 go along with observations of increased CO_2/SO_2 ratios (Table 5 and in Aiuppa et al. (2018)) while Cl/S ratios in 2016 are similar to 2009. Aiuppa et al. (2018) pointed out that the formation of the lava lake was associated with upward magma migration and deep rising CO_2 -rich gas bubbles.

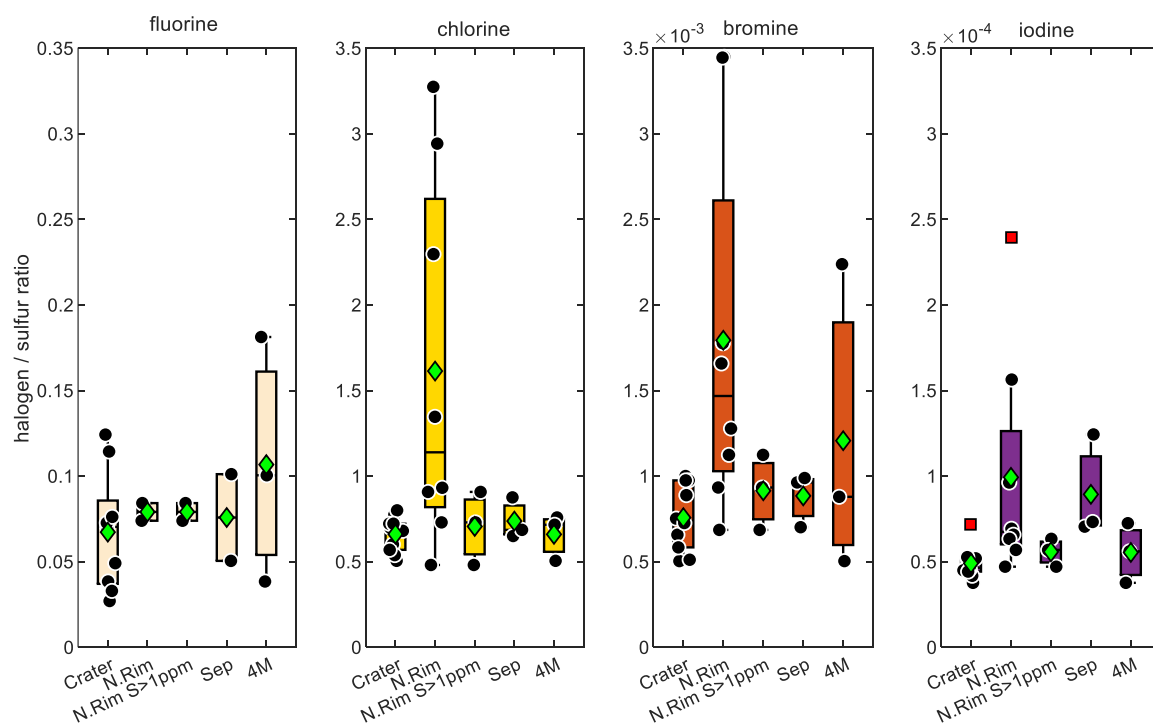


Figure 3: Evaluation of the measured halogen to sulfur ratios – Crater: Raschig tube in July at Santiago crater; N.Rim: RT in July at Nindiri rim; N.Rim S > 1ppmv: RT in July at Nindiri rim without samples with less than 1 ppmv sulfur; Sep: RT in September at Santiago crater; 4M: Drechsel bottle samples in July at Santiago crater with 4 molar NaOH solution; for each box, the black dots are the individual data points, the central mark is the median, the green diamond is the mean, the box extends vertically between the 25th and 75th percentiles, the whiskers extend to the most extreme data that are not considered outliers, and the outliers are plotted individually marked by red squares.



Table 4: Median halogen to sulfur ratios measured at Santiago crater and downwind at Nindirí rim compared with downwind samples from a more dense plume $S > 1$ ppmv; the uncertainty is given as the median average deviation.

	F/S	Cl/S	Br/S	I/S
Crater	0.078 ± 0.028	0.69 ± 0.08	$(7.4 \pm 1.7) \times 10^{-4}$	$(4.6 \pm 1.0) \times 10^{-5}$
Nindirí Rim	0.079 ± 0.005	1.10 ± 0.53	$(15 \pm 4) \times 10^{-4}$	$(6.8 \pm 1.6) \times 10^{-5}$
Nindirí Rim, $S > 1$ ppmv	0.079 ± 0.005	0.73 ± 0.18	$(9.3 \pm 1.9) \times 10^{-4}$	$(5.7 \pm 6.5) \times 10^{-5}$
Crater September	0.076 ± 0.025	0.69 ± 0.04	$(9.6 \pm 0.3) \times 10^{-4}$	$(7.3 \pm 0.3) \times 10^{-5}$
Crater DB 4M	0.10 ± 0.06	0.72 ± 0.04	$(8.8 \pm 3.8) \times 10^{-4}$	$(5.6 \pm 1.6) \times 10^{-5}$

Table 5: Halogen to sulfur and inter-halogen ratios of Masaya's gas emissions between 2006 and 2016.

	Witt et al. 2008	Martin et al. 2010	this study
year	2006	2009	2016
F/S	n.d.	0.13 ± 0.01	0.07 ± 0.03
Cl/S	0.32 ± 0.01	0.77 ± 0.06	0.69 ± 0.07
Br/S	$(2.7 \pm 0.2) \times 10^{-4}$	$(3.2 \pm 1.0) \times 10^{-4}$	$(7.4 \pm 1.7) \times 10^{-4}$
I/S	$(1.8 \pm 0.1) \times 10^{-5}$	$(1.5 \pm 0.2) \times 10^{-5}$	$(4.6 \pm 1.0) \times 10^{-5}$
Cl/F	n.d.	6.0 ± 0.3	9.9 ± 4.1
Cl/Br	$(1.2 \pm 0.1) \times 10^3$	$(2.4 \pm 0.7) \times 10^3$	$(0.9 \pm 0.2) \times 10^3$
Cl/I	$(1.8 \pm 0.1) \times 10^4$	$(5.0 \pm 0.4) \times 10^4$	$(1.5 \pm 0.4) \times 10^4$
$\text{CO}_2/\text{SO}_2^a$	3.4 ± 0.5	$2.7 \pm 0.3^{\#}$	4.0 ± 0.6^b and $3.6 \pm 0.6^{c*}$

Halogen data from Witt et al. and Martin et al. was derived from filter pack measurements; ^a Multi-GAS (MG) data; ^b MG data from (de Moor et al., 2017); ^c MG data from (Rüdiger et al., 2018); [#] OP-FTIR data

5

5.2. Reactive halogens

In the plume of Masaya volcano reactive halogens were measured by gas diffusion denuder sampling. The reactive halogen data are categorized by their sampling location and the median of the species ratios for each location was calculated together with their propagated uncertainties (Table 6). For each location, a distance to the vent was estimated based on path of the downwind drifting plume and GPS data of the sampling locations. For aerial samples the GPS coordinates of the highest measured SO_2 mixing ratios were chosen as a representative location. The uncertainties of the distance were estimated for each location based on the spatial distribution of the respective samples. Figure 4 shows the reactive halogen to sulfur (HalX/S) and reactive halogen to total halogen (HalX/Hal) ratios as a function of the distance to the vent. For bromine, whose activation in volcanic plumes has been studied extensively in the past (e.g., Oppenheimer et al., 2006; Bobrowski et al., 2007; Bobrowski and Platt, 2007; Bobrowski and Giuffrida, 2012), an increase of the BrX/S and BrX/Br over distance and therefore plume age



is clearly observable. The ratio of BrX/S increases from $(1.3 \pm 0.6) \times 10^{-4}$ at the crater rim up to $(20 \pm 14) \times 10^{-4}$ downwind location above the caldera valley (red dots in Figure 1). Also, the BrX/Br ratio increases from 0.20 ± 0.13 at the crater rim to 0.76 ± 0.26 at *Cerro Ventarrón* (purple dot). Those ratios obtained for the crater rim are in the range of what was recently measured at the volcanoes Etna (Rüdiger et al., 2017), Nyamulagira (Bobrowski et al., 2017) and Stromboli (Rüdiger et al., 2018) by the same method and at similar distances from the vents. Although the Br/S ratio increased from 2009 to 2016 the average BrO/SO₂ ratio from August to September 2016, 3.4×10^{-5} , is similar to observations by Kern et al. (2009) (average of 3.0×10^{-5}) who conducted measurements at the crater rim of Santiago crater. Due to technical problems causing instrument outage, DOAS data were only available for the period shortly after the field campaign in July 2016, but we assume that no significant changes in the degassing behavior occurred between July and September 2016, which is plausible regarding the stable CO₂/SO₂ gas ratios presented by Aiuppa et al. (2018) for that period. Therefore, a comparison of the BrO/SO₂ and BrX/S ratios is feasible. For the plume measured by the DOAS instrument in the zenith orientation, we estimated a distance to the vent of 1.4 km and employed wind speed data to derive an estimated plume age, which is presented in Table 7. Due to the nature of several estimations needed to assess the data, it can be argued that in the early plume (< 5 min) BrO accounts for approximately 10 % of the reactive bromine species (see Figure 5). The increase in the BrX/S ratio after 6 minutes needs to be regarded with caution, since the downwind BrX/S ratio was obtained in a diluted plume, which is a source of uncertainty, due to low SO₂ mixing ratios. The denuder sampling enriches reactive species on the coating and therefore achieves a better detection limit with time. The electrochemical sensor signal on the other hand, is limited by the instrumental detection limit and time-integrated SO₂ mixing ratios may not include phases in which SO₂ was present but below the limit of detection (0.1 ppmv). Therefore, SO₂ might be underestimated and the BrX/S ratio might be overestimated in the diluted plume. These uncertainties are included in the error estimation giving by the error bars of this respective sample. The farthest downwind BrX/S ratio was obtained by a calculation that employs the BrX/Br ratio and the total Br/S ratio, the propagation of the respective uncertainty is included in the error bars as well. However, since the uncertainties are known and estimated, the resulting BrX/S progression still provides insights into the chemistry of the plume. The comparison with the BrO/SO₂ ratios underlines the postulated reaction mechanism, in which BrO is an intermediate product that further reacts to form other reactive species as shown by the reaction paths in Table 1. Therefore, BrO could reach a rather steady state of being formed and reacting to other compounds (e.g., Bobrowski and Giuffrida, 2012; Gutmann et al., 2018).

Furthermore, an activation of chlorine was observed, which has also been detected in the past by remote sensing techniques (e.g., Lee et al., 2005; Bobrowski et al., 2007; Donovan et al., 2014; Gliß et al., 2015). Regarding reactive chlorine ClX (Cl₂, ClNO₂, ClNO₃, HOCl, ClO, OCIO) both the ClX/S and the ClX/Cl ratio increase with distance from the vent. While bromine is activated largely, chlorine activation is only observed in the order of 10^{-4} of total chlorine, due to the higher total chlorine abundance ClX, mixing ratios show still similar values as BrX. Roberts (2018) pointed out that the significant Cl activation would only occur if HBr has already been transformed to BrX and therefore the reaction channels R4b, R5b, R6 and R8 would play a more important role, which lead to the activation of chlorine via BrCl and Cl radicals to form ClO with ozone and OCIO from ClO and BrO. Recently, Kern and Lyons (2018) observed a lack of OCIO in the center of a volcanic plume by DOAS



measurements, while it was increased (relative to SO_2) at the edges. They attributed this observation to the incomplete activation of Br in the plume center and dominance of Br_2 formation (R4a) over BrCl formation (R4b) with an undepleted reservoir of particulate Br. However, Kern et al. (2009) did not detect ClO or OCIO in the plume of Masaya close to the vent, but presented a detection limit for ClO/ SO_2 and OCIO/ SO_2 of 5×10^{-3} and 7×10^{-6} , respectively. Since the ClX/S ratios potentially include ClO and OCIO as reactive chlorine species, we applied a calculation by Kern et al. (2009) to compare our results with their detection limit (for long path DOAS). Under the assumption that ClX is made up by ClO, a potential OCIO/ SO_2 ratio of 6.5×10^{-6} was calculated by employing the rate constant and photolysis frequency for the formation and depletion of OCIO at an average SO_2 mixing ratio of 6 ppmv at the crater rim measurement site. With this calculated ratio being below the estimated detection limit for OCIO by Kern et al. (2009) our observations are in agreement with their DOAS measurements conducted in 2007.

Since iodine is the least abundant halogen in volcanic gases, it has not been observed in many previous studies. The detection of reactive iodine in volcanic plumes was limited to one satellite based study of IO (Schönhardt et al., 2017) in the plume of Mt. Kasatochi in 2008. Due to its low abundance, it is challenging to determine iodine in alkaline trap samples as well as in denuder samples. The ratios of activated iodine to activated bromine (0.16 at Santiago crater, 0.12 further downwind) are in the same order of what Schönhardt et al. (2017) presented for the IO/BrO (0.09), and iodine activation shows a similar trend as bromine (Figure 4). The IX/I ratio increases from 0.3 close to the emission source to 0.9 about 10 minutes downwind, while the IX/S ratio increases by a factor of 5 to 10 on the same distance (Table 6).

5.3. Nighttime sample anomaly

One simultaneous denuder and RT sample was taken during a nighttime visit at the crater rim in 2016. This sample shows an anomalous value for reactive chlorine (see Figure 4). The values for reactive bromine and iodine are similar to that one measured at the same location during the day. One possibility is that this value is an artifact caused during sampling or analysis. However, the absolute signal of Cl-TMB on the respective denuder was above the average signal produced by the highest concentrated calibration standard. Therefore, a contamination by a calibration standard during the analysis can be ruled out. Since the sample was measured in triplicate, a random instrument error is also unlikely. A potential contamination during the sampling in the field or in the laboratory by a different chemical compound would have needed to produce the same retention time and m/z ratio as Cl-TMB, which we assume to be unlikely.

A potential explanation for this high reactive chlorine value is the enhancement of chlorine species at night that are otherwise photolyzed at daytime. A fraction of the HalX species is already formed by high-temperature reactions on the surface of the lava lake (e.g., Br_2 , Cl_2) (Martin et al., 2006) and can be measured at the crater rim without involving photochemistry. For example, the HSC equilibrium model (see section 4.1) for bromine speciation at 1000°C gives a Br_2/HBr ratio of 10^{-4} for an air entrainment into plume gas of 2-5%, which is in the range of the nighttime sample. Regarding reactive chlorine, the HSC model predicts a substantial fraction of Cl atoms (0.1 % of HCl). The Cl atoms can react with each other to form Cl_2 by recombination (Hippler and Troe, 1976), which is more than two orders of magnitudes faster than the reaction of Cl with



methane (Bryukov et al., 2002). Therefore, a formation of Cl_2 in the cooled plume gas mixture, after the emission at the lava lake surface and prior to sampling at the crater rim, would induce a larger night time signal compared to the day with photolysis happening.

5 **Table 6:** RHS to sulfur and total halogen ratios at five different locations and estimated plume ages at 5 m/s wind speed, median values, bdl = below detection limit

location ground / air	distance [m]	age [min]	chlorine		bromine		iodine	
			$\text{ClX/S} \times 10^{-4}$	$\text{ClX/Cl} \times 10^{-4}$	$\text{BrX/S} \times 10^{-4}$	BrX/Br	$\text{IX/S} \times 10^{-5}$	IX/I
Santiago rim (g)	217±20	0.7	2.1 ± 0.4	2.7 ± 0.7	1.3 ± 0.6	0.20 ± 0.13	2.1 ± 0.9	0.32 ± 0.15
Nindirí crater (a)	342±50	1.1	3.3 ± 1.0		3.0 ± 0.1		1.1 ± 0.1	
Nindirí rim (g)	737±50	2.5	16 ± 9	11 ± 3	5.0 ± 3.4	0.67 ± 0.05	3.9 ± 1.4	0.31 ± 0.14
Caldera valley (a)	2002±100	6.7	bdl		20 ± 14		11 ± 1	
Cerro Ventarrón (g)	2800±200	9.3	bdl	bdl		0.76 ± 0.26		0.92 ± 0.67

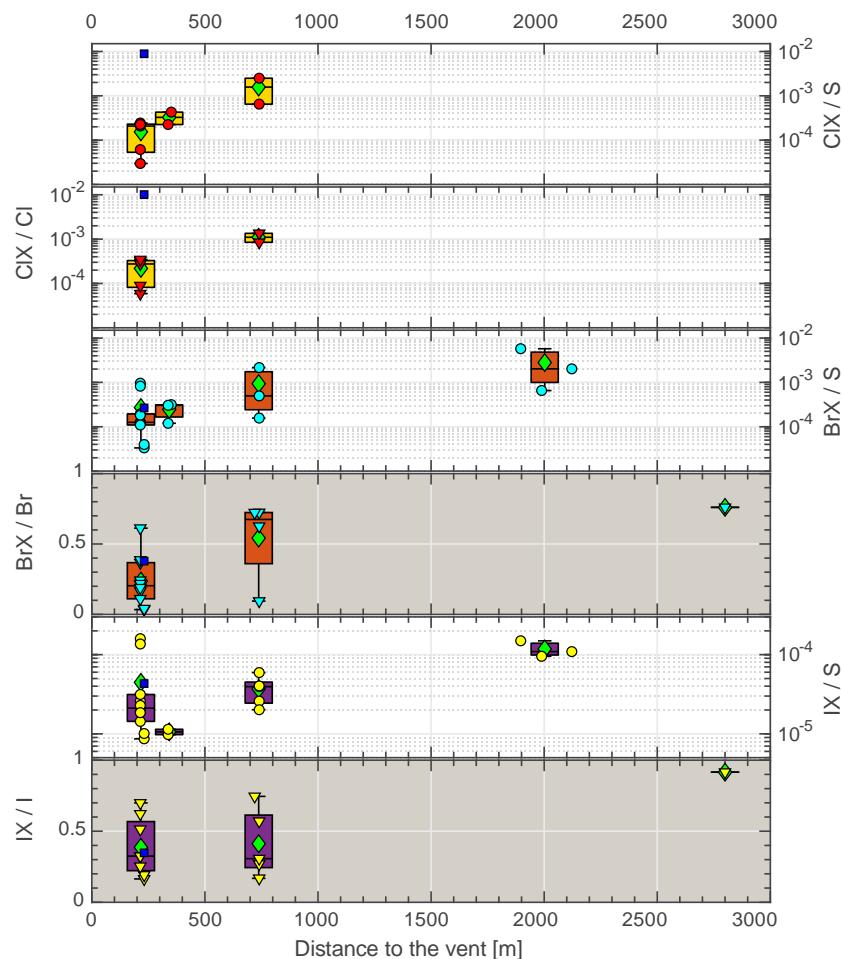


Figure 4: RHS progression during plume aging, mind the non-logarithmic scale with the gray background; circle: Hal/S; triangle: HalX/Hal; diamond: mean; box plot: 25 & 75 percentile and median; blue square: night sample (not included in mean and median calculation).

5 **Table 7:** BrO/SO₂ ratios from a stationary NOVAC DOAS instrument at the estimated plume ages obtained from wind speed (see section 3.5 and supplementary material Figure S2, the values marked with * are single data points).

estimated plume age [min]	average BrO/SO ₂ ratio × 10 ⁻⁵
1.4	0.95*
2.2	3.69*
3.2	2.87 ± 0.31
3.7	2.95 ± 0.56
4.4	2.53 ± 0.75
5.5	2.72 ± 0.83
7.4	3.18 ± 0.83
11.1	3.68 ± 1.22



Table 8: HxO_y and NO_x species used for the initialization of the CAABA/MECCA model runs.

	OH	H_2O_2	HO_2	NO	NO_2
air	7×10^{-13}	0	3×10^{-11}	5×10^{-11}	1×10^{-10}
mag (5:95)	4×10^{-9}	1×10^{-12}	4×10^{-11}	3×10^{-9}	1×10^{-10}
mag (10:90)	5×10^{-9}	2×10^{-12}	4×10^{-11}	8×10^{-9}	1×10^{-10}

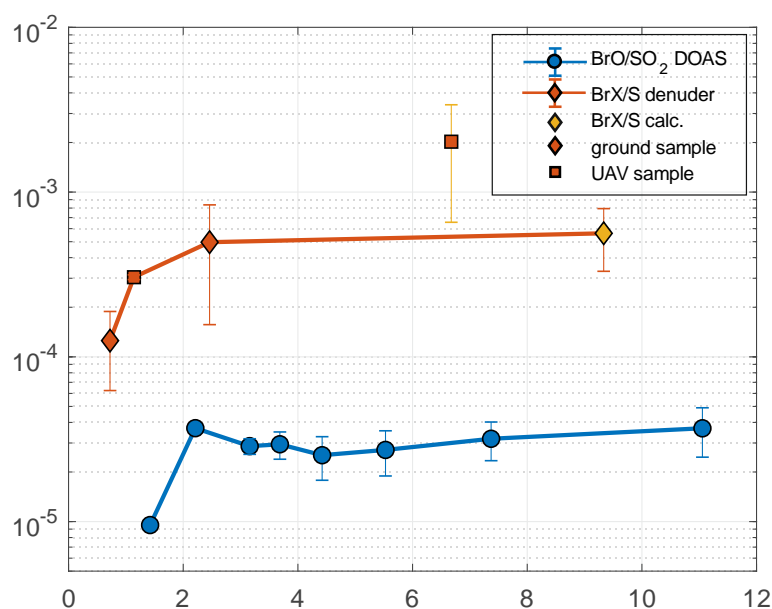


Figure 5: Average RHS/S ratios with plume age: BrO/SO_2 ratios measured by a stationary DOAS instrument and BrX/S ratios obtained by ground- and aerial-based denuder sampling; BrX/S calculated value derived by from BrX/Br ratio at this plume age and crater rim Br/S value. The UAV sample could be affected by underestimation of SO_2 (see text).

5.4. Comparison with box model results

In order to analyze the field observations, a two-stage chemistry modelling approach (see section 4) was conducted. The two major objectives are: (1) investigating the field data for plausibility, and (2) applying the CAABA/MECCA box model in the field of volcanic plume chemistry. The output of the HSC model gives 110 gas species of which 42 were used as input for the CAABA/MECCA box model. By iterating the various parameters for the model start condition that are shown in Table 3, 3816 different model runs of were performed. Each model run simulated the progression of the set of model species during the first 25 minutes. As reactive bromine species are the best studied reactive halogens in volcanic plumes, this section is mostly focused on Br.



5.4.1. Bromine chemistry

The measurement data give the sum of reactive bromine species and the model data provide detailed speciation information. For a comparison of measurement and model, we classify the bromine species into total reactive species $r\text{-Br}$ (Br , Br_2 , BrCl , BrNO_2 , BrNO_3 , HOBr , BrO) and reactive molecular species BrX ($r\text{-Br}$ without Br radical), which are thought to be measured by the denuder coating. The comparison was conducted by a script-based routine, which was required to evaluate the large number of model runs. The routine compares the fit parameters for the progression of the measurement data of BrX/Br and $r\text{-Br}/\text{Br}$ with the respective model speciation output for bromine (see section 4.2 and supplementary Figure S2). Several ensembles of start parameters match the measurement data in good agreement. For the two approaches using either the BrX/Br or the $r\text{-Br}/\text{Br}$ progression, the best matching scenarios are presented in Figure 6 (dashed lines). Furthermore, the BrO/SO_2 progressions were also fitted separately and the best matching model runs with regards to BrO/SO_2 are presented as well (dotted lines). In Figure 6, the solid lines represent those model runs, which show the smallest deviation between the measured data and modelled data for both BrX/Br (or $r\text{-Br}/\text{Br}$) and BrO/SO_2 ratios.

Figure 6 shows the progression of the bromine species over the model time of 25 minutes and the corresponding field measurements. The best matching model scenarios imply atmospheric gas to magmatic gas ratios $V_A:V_M$ of 15:85 or less. Roberts et al. (2014) considered a $V_A:V_M$ of 10:90 or less as likely for system like Etna volcano. For Masaya volcano with its active lava lake, we consider $V_A:V_M$ of up to 15:85 as realistic with respect to the potentially stronger mixing of atmospheric and magmatic gases at the lava lake-atmosphere interface. Besides the initial halogen speciation, changes in $V_A:V_M$ also affect the initial $\text{H}_x\text{O}_y/\text{NO}_x$ mixing ratios (see Table 8). Therefore, best matching model runs are both shown for initial magmatic (red/yellow lines) and atmospheric (blue/purple lines) $\text{H}_x\text{O}_y/\text{NO}_x$ scenarios (magmatic scenario: more $\text{H}_x\text{O}_y/\text{NO}_x$; atmospheric scenario: less $\text{H}_x\text{O}_y/\text{NO}_x$) in Figure 6. Roberts et al. (2014) already discussed the discrepancy between a kinetically limited formation of NO_x from background N_2 and the contradicting observations of $\text{H}_x\text{O}_y/\text{NO}_x$ compounds at the crater rim (e.g., Oppenheimer et al., 2010; Carn et al., 2011). The HSC model might over predict NO_x since its formation is kinetically limited as a result of the high bond strength of N_2 that is entrained in the plume. Roberts et al. (2014) alluded the need for an alternative explanation for NO_x at volcanoes, where it has been observed. In a recent study Roberts et al. (2019) presented a time-resolved chemical kinetics model for the high temperature near source chemistry of volcanic emissions that is an improvement to the HSC model. In contrast to HSC Roberts et al. (2019) reproduced reduced gas species and high temperature formation of HO_2 , OH , and H_2O_2 , but do not include NO_x chemistry yet. Therefore, two scenarios with magmatic and atmospheric $\text{H}_x\text{O}_y/\text{NO}_x$ composition are investigated as extremes, representing the HSC output and the atmospheric background composition, respectively.

For both, the progressions of BrX/Br and $r\text{-Br}/\text{Br}$ as well as BrO/SO_2 ratios, model scenarios with a good agreement to the measurement data have been identified. However, for the BrX/S and $r\text{-Br}/\text{S}$ ratios (Figures 6b, 6f) the model underpredicts the field observations. In the modelled BrX/S and $r\text{-Br}/\text{S}$ ratios the total sulfur content was employed, which is constant, except for dilution. Since the prediction of the BrX/Br and $r\text{-Br}/\text{Br}$ progressions are quite good, the measured BrX/S and $r\text{-Br}/\text{S}$ ratios



could be overestimated, due to an underestimation of sulfur by measuring only SO_2 . This could also be the case when the plume is diluted and SO_2 is below the detection limit of electrochemical sensor. Under these circumstances, the sensor does not detect SO_2 while the denuder is still trapping small amounts of reactive Br, resulting in an overestimated BrX/S (r-Br/S) ratio (see section 5.2).

- 5 The measured BrO/ SO_2 progression (Figures 6c, 6g) could be reproduced by various model runs with different $V_A:V_M$ ratios, $\text{H}_x\text{O}_y/\text{NO}_x$ mixing ratios and initial start concentrations. BrO/ SO_2 ratio is only slightly over predicted in the model runs that fitted best for the BrX/Br progression and in the atmospheric scenario of the r-Br/Br progression. This overprediction is smaller for the model run with the magmatic $\text{H}_x\text{O}_y/\text{NO}_x$ scenario (see Table 8). Potentially, a higher abundance of H_xO_y and NO_x species could promote the loss of BrO to form HOBr and BrNO_3 . A local maximum of BrO in the BrO/ SO_2 progression can
 10 be observed around 2-3 minutes plume age in the model runs that are fitted best for the progression of BrX and r-Br and the one scenario, which fits best for r-Br/Br and BrO/ SO_2 (solid violet line in Fig. 6). The DOAS data with the employed plume age approximation could indicate a small local maximum around the same age, although only a single data point is representing this plume age.

- The model runs that show a good agreement with the BrO/ SO_2 progression (Figures 6c, 6g) are able to reproduce the fraction
 15 of BrO of the total reactive bromine (5-15 %) (Figure 6d, 6h) comparable to what was observed in the field data (~10 %). Employing a conversion of total Br to reactive Br of 67 % for a plume age of 2.5 minutes (Table 6) and a BrO fraction on the BrX of 10 %, BrO accounts in our case for roughly 7 % of the total bromine. Recently Gutmann et al. (2018) compiled data on the extent of the BrO/Br fraction at Masaya and presented values of 5-15 % increasing with the distance to the crater.

- Figure 7 gives an overview on the detailed bromine speciation during the first 25 minutes of the model runs that were fitted
 20 best to the observations of the reactive bromine progression and the BrO/ SO_2 data. For both approaches with and without including Br radicals to the species measured by the denuders one atmospheric and one magmatic scenarios is presented in detail. It is noticeable that the BrCl fraction is more elevated in the scenarios with a magmatic $\text{H}_x\text{O}_y/\text{NO}_x$ composition compared to the atmospheric scenarios, while the Br is less prominent. BrCl is photolyzed slower than Br_2 (Maric et al., 1994), therefore a larger fraction of BrCl, compared to Br_2 , could cause a slower formation of Br. The BrCl fractions might also be
 25 enhanced due to larger abundances of ClX, including ClO, OClO and Cl_2 .

- In Figure 7 the detailed bromine speciation for the best matching model scenarios of Figure 6 are presented. In all four runs, the HBr mixing ratios decrease rapidly after initialization as it is transformed to reactive species or taken up by the aerosol. Less aerosol (particle number concentration and diameter) leads to a slower loss of HBr (Figure 7a). Only a small amount of bromine is present as aqueous $\text{Br}_{(\text{aq})}^-$. Regarding the heterogeneous reaction mechanism of the “bromine explosion”, aqueous
 30 $\text{Br}_{(\text{aq})}^-$ and $\text{HOBr}_{(\text{aq})}$ is needed to form Br_2 , which is then emitted from the particle. In the model, it seems that the formation of Br_2 and its fractionation into the gas phase is faster than the uptake of HBr and HOBr, which leads to depletion of Br in the particles. While the aerosol is poor in bromide and rich in chloride, heterogeneous formation of BrCl by $\text{HOBr}_{(\text{aq})}$ and $\text{Cl}_{(\text{aq})}^-$ represents a sink for $\text{HOBr}_{(\text{aq})}$ and source for BrCl by R4b. Formation of BrCl by the mentioned reaction (R4b) is also known for other systems e.g., simulated ice surfaces (e.g., Fickert et al., 1999; Huff and Abbatt, 2000).



We compared our model study to earlier studies that applied the models MISTRA (von Glasow, 2010) and PlumeChem (Roberts et al., 2014), which were based on volcanic plume measurements at Mt. Etna. All three studies succeed to simulate a bromine activation to the magnitude measured by our denuder sampling technique. However, the differences in the specific species making up BrX or r-Br is substantial. While similar to our results, PlumeChem reproduces a large fraction of Br₂ as well as a local maximum in the young plume (~ 5 min), MISTRA on the other hand shows a constant fraction of approximately 5-10 %. The modelled HOBr in PlumeChem is also in agreement for the first 10 minutes with our CAABA/MECCA output. But regarding BrO, our finding is comparable to results of MISTRA that produces less than 10 % BrO of the total Br in the young plume, while PlumeChem models a varying BrO fraction between 10 % to 50 % of the total Br, depending on the initial total Br/S ratio and BrO reaching a fraction of ~ 50 % of the reactive bromine in all its scenarios. Furthermore, the substantial contribution of BrCl, which we simulated could not be reproduced by MISTRA or PlumeChem. BrNO₃ (formed by BrO and NO₂) on the other hand is present in PlumeChem and CAABA/MECCA, while MISTRA produces BrNO₂ as a reactive bromine-nitrous species. In our model run in Figure 7b the fraction of BrNO₃ is larger compared to the other scenarios, although in the magmatic scenario NO₂ mixing ratios are similar to the atmospheric background. But in the case of Figure 7b, NO is more abundant and can form NO₂ under O₃ consumption to react with BrO to BrNO₃. However, the formation of BrNO₃ is limited by the photo-labile NO₂ and also a competitive reaction of BrO with HO₂, ClO, and itself (R 2a, 2b, 6, 8). In order to explore the reason for those model differences in more detail, the reaction mechanisms used by the three models need to be compared and similarities and differences in reaction rates shall be evaluated. This however lies beyond the objectives of this work.

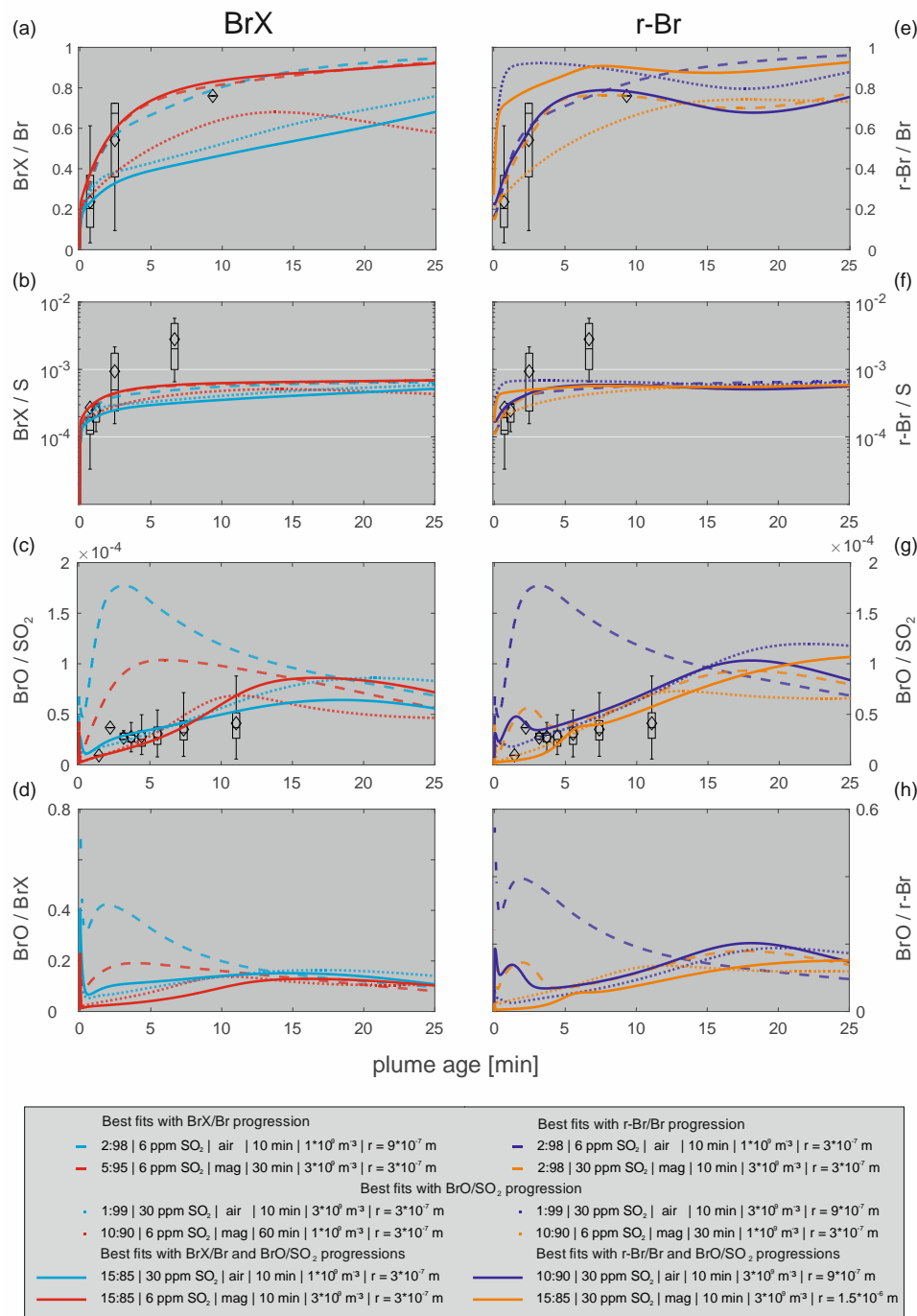


Figure 6: Temporal evolution of different modelled bromine species ratios (molar) over the model time of 25 minutes with the respective measurement data (if available). Each sub-figure shows the model runs for the respective species ratio that are closest to the measurement data, derived by the fit comparison approach described in section 4.2. The legend provides the detailed model parameter ensembles for the respective plots according to the parameters given in Table 3 (#2 to #7).

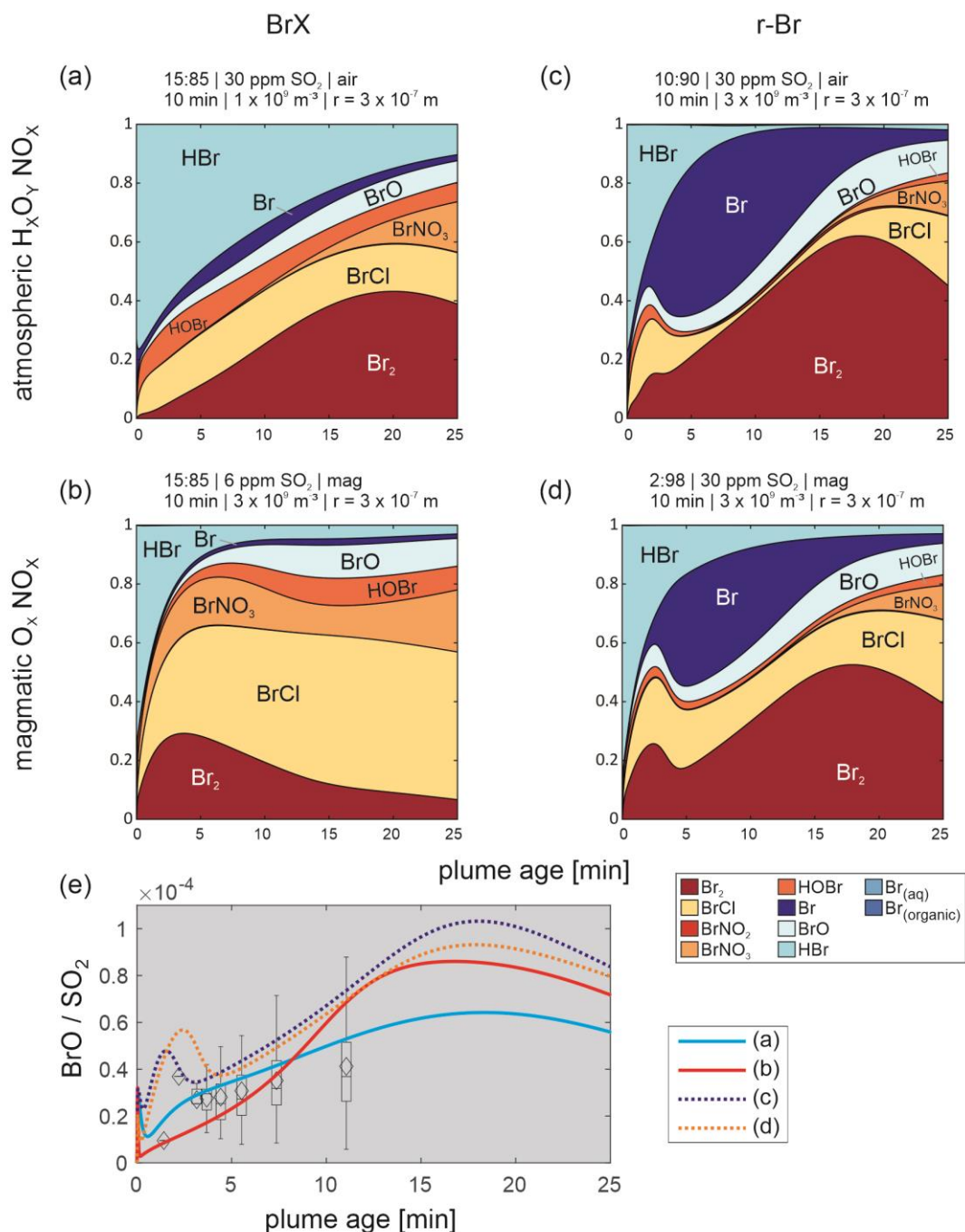


Figure 7: (a-d) Detailed bromine speciation for the first 25 minutes of four selected model runs closest to the measured BrX/Br, r-Br/Br and BrO/SO₂ progressions introduced in Figure 6. Four different model scenarios are shown, that fit best to the measurement data (reactive bromine to total bromine), using the progressions of BrX/Br and r-Br/Br with magmatic and ambient air oxidants amounts respectively; (e) the corresponding BrO/SO₂ ratios to the model runs of (a-d).



5.4.2. Input parameter sensitivity analysis

The so-called base run of CAABA/MECCA box model, which encompasses the set of parameters from Table 3 that produced the most proximal model recreation to the field observations of the BrX/Br and r-Br/Br ratios, was chosen to study sensitivity of the model with regards on changes of initial start conditions. These start conditions are:

- 5 (1) the initial volume ratio of atmospheric gas to magmatic gas ($V_A:V_M$)
- (2) the quenching factor (QF) for the initial quenching of the mixture of high-temperature gases to low temperature conditions with ambient air (e.g., quenching to 6 ppmv SO₂)
- (3) the dilution time (τ) of the plume, within the initial mixing ratio of an inert species gets diluted by a factor of 1/e (0.37).
- 10 (4) the quantity of reactive oxidants H_xO_y and NO_x
- (5) the number concentration (NC) of particles per m³
- (6) the radii of the particles

The model run shown in Figure 7c was chosen as the model base run. This is based on two considerations. First, an atmospheric H_xO_y/NO_x scenario is more likely than a magmatic scenario due to the kinetically limited formation of NO_x species by high
 15 temperature chemistry in the “effective source region”. Secondly, even though the potential measurement of Br radicals by the denuder technique cannot be ruled out the discrepancy between the r-Br/Br progression and the BrX/Br progression in Figure 7c is still within the deviation of the measurement data. Therefore, the base run (best fit in Figure 7 with the r-Br/Br progression (10:90 | 30 ppmv SO₂ | air | 10 min | 3×10⁹ part. m⁻³ | $r = 3 \times 10^{-7}$)) was used with permuted start conditions to evaluate the influence of these conditions on the specific model outcome. The results of these tests are shown in Figure 8.

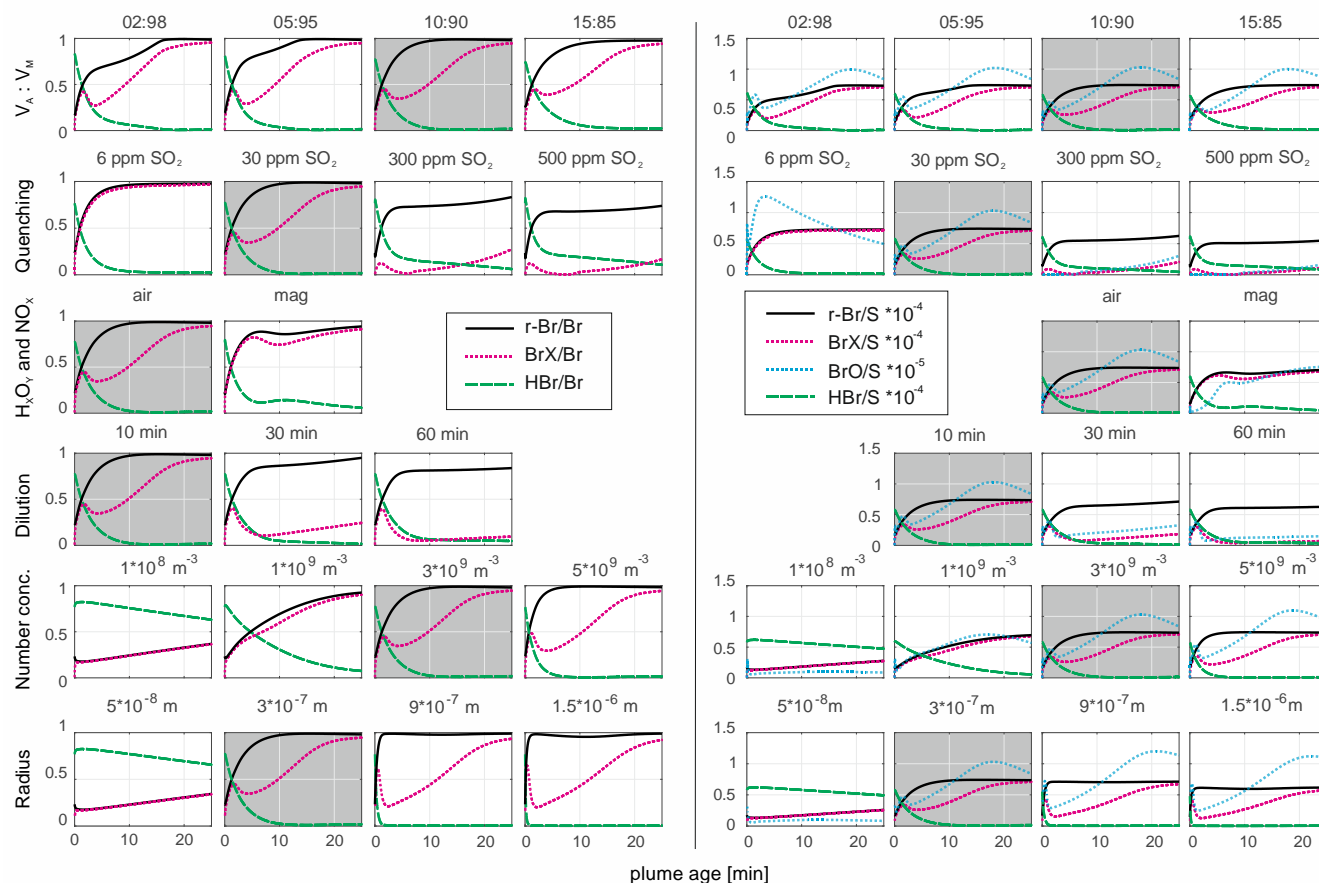


Figure 8: Progression over a model runtime of 25 minutes of selected bromine species related to total bromine (left) and sulfur (right) abundances. The best fit to the measurement data from Figure 7 (c) (10:90 | 30 ppmv SO₂ | air | 10 min | 3×10⁹ part. m⁻³ | r = 3×10⁻⁷ m) is shown with gray background. Within the specific rows the respective model parameter is varied by different values in order to explore the model output answer to the model input change.

Changes in the initial $V_A:V_M$ ratio (in the case of $V_M \geq 85\%$) has only little effect on the BrX/Br or BrX/S ratios, while $r-Br/Br$ is slightly smaller for $V_M \geq 95\%$. There, potentially less Br radical is formed with less atmospheric gas in the HSC model. The QF shows a significant impact, in the base run a quenching to 30 ppmv SO₂ reduces the presence of Br radicals and almost equals $r-Br$ and BrX . Less quenching, indicated by higher SO₂ mixing ratios, leads to less $r-Br$ formation (relative to total Br) and increases the fraction of Br radicals. The relative BrO abundance is also reduced with less quenching due to the larger abundance of bromine in the modelled scenario, while the O₃ entrainment stays fixed. Therefore, more Br is available to consume the same amount of O₃, resulting in less relative formation of BrX . Likewise, a slower dilution results in slower in-mixing of O₃ into the plume and causing the modelled BrX and BrO to be less produced on the same timescale. The shape of the BrX species progression in the scenarios with less quenching (30 to 500 ppmv SO₂) and slower dilution time (30 and 60 minutes) are related to a substantial consumption of ozone in the modelled plume (see Figure S4). In the 30 ppmv SO₂ scenario, ozone is decimated almost completely already at around 2 minutes after plume release, causing a temporarily decrease of BrX .



followed by an increase while the ozone concentration recovers. With a quenching to 6 ppm SO₂ sufficient O₃ is provided which results in the almost complete reaction of Br radicals to other BrX species. The scenarios with 300 and 500 ppmv SO₂ show a rather complete depletion of ozone during the simulation time. A dilution time of 10 minutes (to a factor of 1/e (0.37) of the initial mixing ratio) fits best to the measured average SO₂ mixing ratios in the aged plume.

5 With an initial magmatic H_xO_y/NO_x abundance r-Br consists of less Br radicals and more other BrX species. The presence of NO_x (Figure S4) promotes the formation of reactive bromine reservoir species and causes less ozone consumption compared to the atmospheric H_xO_y/NO_x case. The aerosol number concentration (NC) at a given aerosol size, does affect the Br activation in a way that with a certain threshold enough aerosol particles respectively aerosol surface or volume are present that the Br activation is not limited by this parameter. This is also true for the radius of the aerosol particles at the number

10 concentration of the base run. Regarding the base run scenario, a surface area of $3.4 \times 10^{-3} \text{ m}^2/\text{m}^3$ (3×10^9 particles m⁻³ at 300 nm radius) appears to be appropriate for the observed Br activation. Otherwise, less particles with the same radius leads to a slower activation similar to the same number of smaller particles. However, a larger surface area per volume leads to an increased activation pace. Similar to our observations Roberts et al. (2014) showed the impact of higher and lower aerosol surface on the Br activation, leading to larger and smaller activation respectively, in their PlumeChem model. However, the

15 necessary surface area is easily provided by the volcanic aerosol at Masaya considering the obtained optical particle counter data on the particle sizes and abundances, which raised up to approximately $1.5 \times 10^{-2} \text{ m}^2/\text{m}^3$ calculated with data from Stix et al. (2018).

5.4.3. Chlorine and iodine chemistry

The HSC model produces reactive chlorine and iodine species. A typical output for chlorine is a Cl₂/Cl ratio of 8×10^{-5} and

20 ClO/Cl of 3×10^{-6} . ClONO₂ and OCIO are formed over the model run time and the measured reactive chlorine species are in the order of the model predictions ($\sim 0.3 \times 10^{-3}$ at 2-3 minutes), although the model base run shows a decrease of reactive species during the first 7-8 minutes (see Figure 9). During the first 5 minutes, the modelled OCIO/SO₂ ratios (Figure 9d) are in the order ($\sim 2 \times 10^{-5}$) of PlumeChem results by Roberts et al. (2018), who compared their simulations with measurements of Gliß et al. (2015). Both, ClO and OCIO, decrease around 10 minutes, which is about the same plume age where modeled BrCl has a

25 minimum compared to BrX.

Regarding iodine, the modelled speciation reflects the field observations, albeit only partially. Similar to Martin et al. (2006), 99 % of the iodine is present as atomic I in the HSC model. Diatomic iodine species are formed during the first minute of the box model simulation alongside HOI by reactions of analogous to R1 and R2. Eventually IO is further oxidized similar to R8 to form OIO, that is known to condense on preexisting particles and undergo new particle formation (e.g., Hoffmann et al.,

30 2001; O'Dowd et al., 2002; Saiz-Lopez et al., 2012). CAABA/MECCA assumes a loss rate of OIO for new particle formation and uptake on existing aerosol that is combine to I_xO_{y(aq)}. The kinetics of this process and the fate of the respective iodine species are not constrained very well. However, our measurements suggest a reactive iodine fraction (IX: I₂, IO, INO₂, IONO₂, HOI, OIO, HIO₃, ICl, IBr; r-I: IX + I) of 0.32 ± 0.15 (0.16 to 0.70) at the crater rim which is in agreement with the model result.

For a more distant position the measurements and the model diverge (Figure 9b), though potentially a smaller loss rate of OIO and further aqueous chemistry of $I_xO_y(aq)$ could explain the measured reactive iodine species downwind. Furthermore, ultrafine and newly formed particles ($<10\text{nm}$) consisting of I_xO_y could also diffuse to the denuder walls and react with the coating and therefore induce a reactive iodine signal.

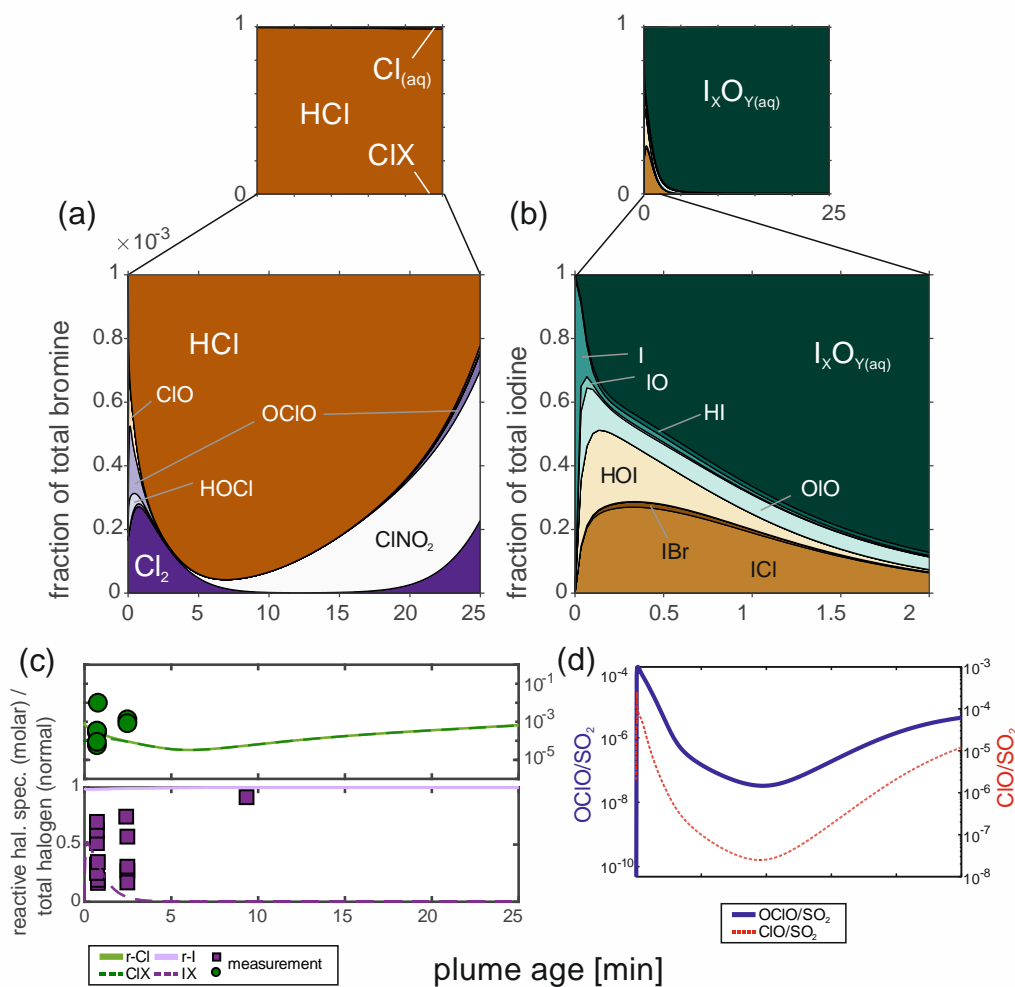


Figure 9: (a) Chlorine and (b) iodine speciation of the base model run (10:90 | 30 ppmv SO_2 | air | 10 min | 3×10^9 part. m^{-3} | $r = 3 \times 10^{-7}$ m); (c) comparison of the measured and modelled reactive halogen to total; (d) molar $OCIO/SO_2$ and ClO/SO_2 ratios.



6. Conclusion and outlook

In this study, we present a combination of ground-based and UAV-based measurements of halogen speciation in the plume of Masaya volcano over an estimated plume age of 1-11 minutes. The application of an UAV enabled us to sample the plume at an age that is typically not accessible. The application of various techniques enabled the most detailed observation of changes in the halogen speciation over this timescale. Further, the employment of the CAABA/MECCA box model enabled the assessment and investigation of additional non-directly observed parameters – ozone entrainment into the plume (quenching and plume dilution) and $\text{H}_x\text{O}_y/\text{NO}_x$, which drive the activation of bromine primarily. The rapid increase of reactive bromine species during the first few minutes was observed by gas diffusion denuder sampling as well as by DOAS measurements of BrO, which is an intermediate product of the autocatalytic activation cycle. At Masaya the BrO/ SO_2 reached a plateau as has been observed at other volcanoes (Platt and Bobrowski, 2015) and in model simulations (Roberts et al., 2014). After approximately 10 minutes, the sum of reactive bromine species (r-Br) accounted for 76 % of the total bromine and BrO roughly contributes up to 10 % of r-Br in the first few minutes. The BrO contribution to r-Br, estimated by measurement data, was reproduced to a large extent by the box model simulations. The overall progression of the BrX/Br and r-Br/Br ratios were reflected by various model runs encompassing different plausible starting parameters. The knowledge of further data on O_3 , H_xO_y and NO_x in the plume would help to pin point a more detailed set of start parameters. A discrepancy of the modelled and measured BrX/S (and r-Br/S) ratios could be caused by underestimation of SO_2 in the electrochemical sensor data for the diluted plume. The box model simulations with a set of plausible initial parameters nicely reproduce the observations of the relative bromine speciation measured by RT and denuders. The measured and modelled chlorine speciation are only comparable during the first 2-3 minutes of the model run due to limited observational data. Furthermore, the implementations of iodine chemistry such as the knowledge on iodine oxide particle formation into the model are necessary to enable a qualified comparison with the observed iodine data. Although the bromine activation was reproduced by CAABA/MECCA, differences of reactive bromine to sulfur ratios occurred between observations and model. Therefore, a further knowledge of the chemical mechanism towards volcanic plumes environments is still needed alongside more detailed observational studies. However, a first application of CAABA/MECCA in this field provided us with a possible explanation of our field data. Within the range of model parameters that we studied, the dilution time and the quenching factor for the model runs showed to have large effect while the initial volume ratio of atmospheric and magmatic gases (in the HSC model) seems to play only a less important role. The presence of initial oxidants showed to influence the relative abundance of the different Br species (e.g., Br_2 , BrCl, BrNO_3 , BrO, Br), while not largely affecting the overall reactive bromine abundance. In model runs with a slower dilution or larger initial Br presence, ozone in-mixing seems to be a limiting factor for the bromine activation. Although we do not have field data for ozone concentrations, the observed dilution over 10 minutes suggests the presence of sufficient in-mixed air and therefore O_3 .

Chlorine activation was observed to an extent of about 0.1% of total chlorine while reactive iodine was measured to make up roughly 30% of total iodine in the first few minutes and is almost completely converted over the observed timescale.



Our method achieved to determine the sum of reactive species for the respective halogens and the detailed speciation within the reactive fraction is a topic of future research. Therefore, other selective denuder coatings will be developed and applied to further distinguish between species such as Br₂, BrCl or BrNO₃ and Br radicals. Although we estimated that BrO contributes up to 10 % of r-Br in the first few minutes and r-Br accounts for up to 76% of total Br after 10 minutes, but less in the early
5 plume. The BrO formation seems to be more sensitive to changing model parameters than the overall r-Br formation. Since BrO detection is possible with DOAS spectrometers and has already been conducted at numerous volcanoes, the influencing factors on the extent of its formation need to be studied further, also with regards to estimating total bromine emissions and variations with volcanic activity. Detailed measurements in the field and further studies in controlled environments like atmospheric simulation chambers will help to further assess bromine activation in volcanic plumes.

Author contributions.

JR, NB and TH designed the research. JR, AG, NB, JMdm, MI, MM, AF and JS performed field sample and data collection. JR, AG, ML conducted laboratory sample analyses. FD provided the BrO/SO₂ NOVAC results. JR, JLT, AS, EM, JV and JMC provided instrumental and logistical support. RS provided the CAABA/MECCA program and helped to perform model
15 runs. All authors contributed to the manuscript.

Competing interests

The authors declare that they have no conflict of interest.

Acknowledgments

JR, NB, AG and TH acknowledge support by the research center “Volcanoes and Atmosphere in Magmatic, Open Systems” (VAMOS) at the University of Mainz, Germany. JR is thankful for funding from the German Academic Exchange Service (DAAD) and the support by INETER (Nicaragua) and OVSICORI Universidad Nacional (Costa Rica). JR and NB thank also the DFG project “HALVIRE” (BO 3611/2-1, HE 5214/8-1, PL 193/18-1) for financial support during data evaluation, modelling and writing. Our thanks also to Dr. Feiyue Wang from the Centre for Earth Observation Science (CEOS) and the
25 Department of Environment and Geography of the University of Manitoba Canada, for supporting field work at the Masaya complex.



References

- Aiuppa, A.: Degassing of halogens from basaltic volcanism: Insights from volcanic gas observations, *Chemical Geology*, 263, 99–109, doi:10.1016/j.chemgeo.2008.08.022, 2009.
- Aiuppa, A., Baker, D. R., and Webster, J. D.: Halogens in volcanic systems, *Chemical Geology*, 263, 1–18, doi:10.1016/j.chemgeo.2008.10.005, 2009.
- Aiuppa, A., Federico, C., Franco, A., Giudice, G., Gurrieri, S., Inguaggiato, S., Liuzzo, M., McGonigle, A. J. S., and Valenza, M.: Emission of bromine and iodine from Mount Etna volcano, *Geochemistry, Geophysics, Geosystems*, 6, n/a-n/a, doi:10.1029/2005GC000965, 2005.
- Aiuppa, A., Federico, C., Giudice, G., Gurrieri, S., Liuzzo, M., Shinohara, H., Favara, R., and Valenza, M.: Rates of carbon dioxide plume degassing from Mount Etna volcano, *Journal of Geophysical Research: Solid Earth*, 111, doi:10.1029/2006JB004307, 2006.
- Aiuppa, A., Moor, J. M. de, Arellano, S., Coppola, D., Francofonte, V., Galle, B., Giudice, G., Liuzzo, M., Mendoza, E., Saballos, A., Tamburello, G., Battaglia, A., Bitetto, M., Gurrieri, S., Laiolo, M., Mastrolia, A., and Moretti, R.: Tracking Formation of a Lava Lake From Ground and Space: Masaya Volcano (Nicaragua), 2014–2017, *Geochemistry, Geophysics, Geosystems*, 19, 496–515, doi:10.1002/2017GC007227, 2018.
- Aiuppa, A., Moretti, R., Federico, C., Giudice, G., Gurrieri, S., Liuzzo, M., Papale, P., Shinohara, H., and Valenza, M.: Forecasting Etna eruptions by real-time observation of volcanic gas composition, *Geology*, 35, 1115–1118, doi:10.1130/G24149A.1, 2007.
- Bobrowski, N. and Giuffrida, G.: Bromine monoxide/sulphur dioxide ratios in relation to volcanological observations at Mt. Etna 2006–2009, *Solid Earth*, 3, 433, 2012.
- Bobrowski, N., Giuffrida, G. B., Arellano, S., Yalire, M., Liotta, M., Brusca, L., Calabrese, S., Scaglione, S., Rüdiger, J., Castro, J. M., Galle, B., and Tedesco, D.: Plume composition and volatile flux of Nyamulagira volcano, Democratic Republic of Congo, during birth and evolution of the lava lake, 2014–2015, *Bulletin of Volcanology*, 79, B09207, doi:10.1007/s00445-017-1174-0, 2017.
- Bobrowski, N., Glasow, R. von, Aiuppa, A., Inguaggiato, S., Louban, I., Ibrahim, O. W., and Platt, U.: Reactive halogen chemistry in volcanic plumes, *Journal of Geophysical Research*, 112, doi:10.1029/2006JD007206, 2007.
- Bobrowski, N., Hönninger, G., Galle, B., and Platt, U.: Detection of bromine monoxide in a volcanic plume, *Nature*, 423, 273–276, 2003.
- Bobrowski, N. and Platt, U.: SO₂/BrO ratios studied in five volcanic plumes, *Journal of Volcanology and Geothermal Research*, 166, 147–160, 2007.
- Bryukov, M. G., Slagle, I. R., and Knyazev, V. D.: Kinetics of Reactions of Cl Atoms with Methane and Chlorinated Methanes, *The Journal of Physical Chemistry A*, 106, 10532–10542, doi:10.1021/jp0257909, 2002.



- Burton, M. R., Oppenheimer, C., Horrocks, L. A., and Francis, P. W.: Remote sensing of CO₂ and H₂O emission rates from Masaya volcano, Nicaragua, *Geology*, 28, 915–918, doi:10.1130/0091-7613(2000)28<915:RSOCAH>2.0.CO;2, 2000.
- Burton, M. R., Mader, H. M., and Polacci, M.: The role of gas percolation in quiescent degassing of persistently active basaltic volcanoes, *Earth and Planetary Science Letters*, 264, 46–60, doi:10.1016/j.epsl.2007.08.028, 2007.
- 5 Cadoux, A., Iacono-Marziano, G., Scaillet, B., Aiuppa, A., Mather, T. A., Pyle, D. M., Deloule, E., Gennaro, E., and Paonita, A.: The role of melt composition on aqueous fluid vs. silicate melt partitioning of bromine in magmas, *Earth and Planetary Science Letters*, 498, 450–463, doi:10.1016/j.epsl.2018.06.038, 2018.
- Carn, S. A., Clarisse, L., and Prata, A. J.: Multi-decadal satellite measurements of global volcanic degassing, *Journal of Volcanology and Geothermal Research*, 311, 99–134, doi:10.1016/j.jvolgeores.2016.01.002, 2016.
- 10 Carn, S. A., Fioletov, V. E., McLinden, C. A., Li, C., and Krotkov, N. A.: A decade of global volcanic SO₂ emissions measured from space, *Scientific reports*, 7, 44095, doi:10.1038/srep44095, 2017.
- Carn, S. A., Froyd, K. D., Anderson, B. E., Wennberg, P., Crounse, J., Spencer, K., Dibb, J. E., Krotkov, N. A., Browell, E. V., Hair, J. W., Diskin, G., Sachse, G., and Vay, S. A.: In situ measurements of tropospheric volcanic plumes in Ecuador and Colombia during TC 4, *Journal of Geophysical Research*, 116, 86, doi:10.1029/2010JD014718, 2011.
- 15 Carroll, R. and Holloway, J. R.: Volatiles in magmas, *Reviews in mineralogy*, op. 1994.
- de Moor, J. M., Aiuppa, A., Avar, G., Wehrmann, H., Dunbar, N., Muller, C., Tamburello, G., Giudice, G., Liuzzo, M., Moretti, R., Conde, V., and Galle, B.: Turmoil at Turrialba Volcano (Costa Rica): Degassing and eruptive processes inferred from high-frequency gas monitoring, *Journal of geophysical research. Solid earth*, 121, 5761–5775, doi:10.1002/2016JB013150, 2016.
- 20 de Moor, J. M., Fischer, T. P., Sharp, Z. D., King, P. L., Wilke, M., Botcharnikov, R. E., Cottrell, E., Zelenski, M., Marty, B., Klimm, K., Rivard, C., Ayalew, D., Ramirez, C., and Kelley, K. A.: Sulfur degassing at Erta Ale (Ethiopia) and Masaya (Nicaragua) volcanoes: Implications for degassing processes and oxygen fugacities of basaltic systems, *Geochemistry, Geophysics, Geosystems*, 14, 4076–4108, doi:10.1002/ggge.20255, 2013.
- de Moor, J. M., Kern, C., Avar, G., Muller, C., Aiuppa, A., Saballos, A., Ibarra, M., LaFemina, P., Protti, M., and Fischer, T. P.: A New Sulfur and Carbon Degassing Inventory for the Southern Central American Volcanic Arc: The Importance of Accurate Time-Series Datasets and Possible Tectonic Processes Responsible for Temporal Variations in Arc-Scale Volatile Emissions, *Geochemistry, Geophysics, Geosystems*, doi:10.1002/2017GC007141, 2017.
- 25 Delmelle, P., Stix, J., Baxter, P., Garcia-Alvarez, J., and Barquero, J.: Atmospheric dispersion, environmental effects and potential health hazard associated with the low-altitude gas plume of Masaya volcano, Nicaragua, *Bulletin of Volcanology*, 64, 423–434, doi:10.1007/s00445-002-0221-6, 2002.
- 30 Diaz, J. A., Pieri, D., Wright, K., Sorensen, P., Kline-Shoder, R., Arkin, C. R., Fladeland, M., Bland, G., Buongiorno, M. F., Ramirez, C., Corrales, E., Alan, A., Alegria, O., Diaz, D., and Linick, J.: Unmanned aerial mass spectrometer systems for in-situ volcanic plume analysis, *Journal of the American Society for Mass Spectrometry*, 26, 292–304, doi:10.1007/s13361-014-1058-x, 2015.



- Dinger, F., Bobrowski, N., Warnach, S., Bredemeyer, S., Hidalgo, S., Arellano, S., Galle, B., Platt, U., and Wagner, T.: Periodicity in the BrO/SO₂; molar ratios in the volcanic gas plume of Cotopaxi and its correlation with the Earth tides during the eruption in 2015, *Solid Earth*, 9, 247–266, doi:10.5194/se-9-247-2018, 2018.
- Dinger, F.: On long-term variations in the BrO/SO₂ molar ratios in volcanic gas plumes, Johannes Gutenberg-University Mainz, 2019. https://publications.ub.uni-mainz.de/theses/frontdoor.php?source_opus=100003100&la=de
- Donovan, A., Tsanev, V., Oppenheimer, C., and Edmonds, M.: Reactive halogens (BrO and OCIO) detected in the plume of Soufrière Hills Volcano during an eruption hiatus, *Geochemistry Geophysics Geosystems*, 15, 3346–3363, doi:10.1002/2014GC005419, 2014.
- Duffell, H. J., Oppenheimer, C., Pyle, D. M., Galle, B., McGonigle, A. J. S., and Burton, M. R.: Changes in gas composition prior to a minor explosive eruption at Masaya volcano, Nicaragua, *Journal of Volcanology and Geothermal Research*, 126, 327–339, doi:10.1016/S0377-0273(03)00156-2, 2003.
- Fickert, S., Adams, J. W., and Crowley, J. N.: Activation of Br₂ and BrCl via uptake of HOBr onto aqueous salt solutions, *Journal of Geophysical Research: Atmospheres*, 104, 23719–23727, doi:10.1029/1999JD900359, 1999.
- Galle, B., Johansson, M., Rivera, C., Zhang, Y., Kihlman, M., Kern, C., Lehmann, T., Platt, U., Arellano, S., and Hidalgo, S.: Network for Observation of Volcanic and Atmospheric Change (NOVAC)—A global network for volcanic gas monitoring: Network layout and instrument description, *Journal of Geophysical Research*, 115, 151, doi:10.1029/2009JD011823, 2010.
- General, S., Bobrowski, N., Pöhler, D., Weber, K., Fischer, C., and Platt, U.: Airborne I-DOAS measurements at Mt. Etna: BrO and OCIO evolution in the plume, *Journal of Volcanology and Geothermal Research*, 300, 175–186, doi:10.1016/j.jvolgeores.2014.05.012, 2015.
- Gerlach, T. M.: Volcanic sources of tropospheric ozone-depleting trace gases, *Geochemistry, Geophysics, Geosystems*, 5,, doi:10.1029/2004GC000747, 2004.
- Giggenbach, W. F.: Variations in the carbon, sulfur and chlorine contents of volcanic gas discharges from White Island, New Zealand, *Bulletin of Volcanology*, 39, 15–27, doi:10.1007/BF02596943, 1975.
- Gliß, J., Bobrowski, N., Vogel, L., Pöhler, D., and Platt, U.: OCIO and BrO observations in the volcanic plume of Mt. Etna – implications on the chemistry of chlorine and bromine species in volcanic plumes, *Atmospheric Chemistry and Physics*, 15, 5659–5681, doi:10.5194/acp-15-5659-2015, 2015.
- Gutmann, A., Bobrowski, N., Roberts, T., Rüdiger, J., and Hoffmann, T.: Advances in bromine speciation in volcanic plumes, *Front. Earth Sci.*, 6, 213, doi:10.3389/feart.2018.00213, 2018.
- Hippler, H. and Troe, J.: Flash photolysis study of the recombination of chlorine atoms in the presence of various inert gases and NO, *International journal of chemical kinetics*, 8, 501–510, doi:10.1002/kin.550080404, 1976.
- Hobbs, P. V., Tuell, J. P., Hegg, D. A., Radke, L. F., and Eltgroth, M. W.: Particles and gases in the emissions from the 1980–1981 volcanic eruptions of Mt. St. Helens, *Journal of Geophysical Research*, 87, 11062, doi:10.1029/JC087iC13p11062, 1982.



- Hoffmann, T., O'Dowd, C. D., and Seinfeld, J. H.: Iodine oxide homogeneous nucleation: An explanation for coastal new particle production, *Geophysical Research Letters*, 28, 1949–1952, doi:10.1029/2000GL012399, 2001.
- Huff, A. K. and Abbatt, J. P. D.: Gas-Phase Br₂ Production in Heterogeneous Reactions of Cl₂, HOCl, and BrCl with Halide–Ice Surfaces, *The Journal of Physical Chemistry A*, 104, 7284–7293, doi:10.1021/jp001155w, 2000.
- 5 Iowa State University: Iowa Environmental Mesonet: ASOS-AWOS-METAR Data:
https://mesonet.agron.iastate.edu/request/download.phtml?network=NI__ASOS, last access: 20 October 2018.
- Jourdain, L., Roberts, T. J., Pirre, M., and Josse, B.: Modeling the reactive halogen plume from Ambrym and its impact on the troposphere with the CCATT-BRAMS mesoscale model, *Atmospheric Chemistry and Physics*, 16, 12099–12125, doi:10.5194/acp-16-12099-2016, 2016.
- 10 Kelly, P. J., Kern, C., Roberts, T. J., Lopez, T., Werner, C., and Aiuppa, A.: Rapid chemical evolution of tropospheric volcanic emissions from Redoubt Volcano, Alaska, based on observations of ozone and halogen-containing gases, *Journal of Volcanology and Geothermal Research*, 259, 317–333, doi:10.1016/j.jvolgeores.2012.04.023, 2013.
- Kern, C. and Lyons, J. J.: Spatial distribution of halogen oxides in the plume of Mount Pagan volcano, Mariana Islands, *Geophysical Research Letters*, doi:10.1029/2018GL079245, 2018.
- 15 Kern, C., Sihler, H., Vogel, L., Rivera, C., Herrera, M., and Platt, U.: Halogen oxide measurements at Masaya Volcano, Nicaragua using active long path differential optical absorption spectroscopy, *Bulletin of Volcanology*, 71, 659–670, doi:10.1007/s00445-008-0252-8, 2009.
- Laaksonen, A., Korhonen, P., Kulmala, M., and Charlson, R. J.: Modification of the Köhler Equation to Include Soluble Trace Gases and Slightly Soluble Substances, *Journal of the Atmospheric Sciences*, 55, 853–862, doi:10.1175/1520-0469(1998)055<0853:MOTKHE>2.0.CO;2, 1998.
- 20 Lee, C., Kim, Y. J., Tanimoto, H., Bobrowski, N., Platt, U., Mori, T., Yamamoto, K., and Hong, C. S.: High ClO and ozone depletion observed in the plume of Sakurajima volcano, Japan, *Geophysical Research Letters*, 32, 2005.
- Liotta, M., Rizzo, A., Paonita, A., Caracausi, A., and Martelli, M.: Sulfur isotopic compositions of fumarolic and plume gases at Mount Etna (Italy) and inferences on their magmatic source, *Geochemistry Geophysics Geosystems*, 13, doi:10.1029/2012GC004118, 2012.
- 25 Louban, I., Bobrowski, N., Rouwet, D., Inguaggiato, S., and Platt, U.: Imaging DOAS for volcanological applications, *Bulletin of Volcanology*, 71, 753–765, doi:10.1007/s00445-008-0262-6, 2009.
- Lübcke, P., Bobrowski, N., Arellano, S., Galle, B., Garzón, G., Vogel, L., and Platt, U.: BrO/SO₂ molar ratios from scanning DOAS measurements in the NOVAC network, *Solid Earth*, 5, 409–424, doi:10.5194/se-5-409-2014, 2014.
- 30 Maric et al.: A study of the UV—visible absorption spectra of Br₂ and BrCl, *Journal of Photochemistry and Photobiology A: Chemistry*, 83, 179–192, doi:10.1016/1010-6030(94)03823-6, 1994.
- Martin, R. S., Mather, T. A., and Pyle, D. M.: High-temperature mixtures of magmatic and atmospheric gases, *Geochemistry, Geophysics, Geosystems*, 7, doi:10.1029/2005GC001186, 2006.



- Martin, R. S., Sawyer, G. M., Spampinato, L., Salerno, G. G., Ramirez, C., Ilyinskaya, E., Witt, M. L. I., Mather, T. A., Watson, I. M., Phillips, J. C., and Oppenheimer, C.: A total volatile inventory for Masaya Volcano, Nicaragua, *Journal of Geophysical Research*, 115, doi:10.1029/2010JB007480, 2010.
- McBirney, A. R.: The Nicaraguan volcano Masaya and its caldera, *Transactions, American Geophysical Union*, 37, 83,
 5 doi:10.1029/TR037i001p00083, 1956.
- McGonigle, A. J. S., Aiuppa, A., Giudice, G., Tamburello, G., Hodson, A. J., and Gurrieri, S.: Unmanned aerial vehicle measurements of volcanic carbon dioxide fluxes, *Geophysical Research Letters*, 35, doi:10.1029/2007GL032508, 2008.
- McGonigle, A. J. S., Delmelle, P., Oppenheimer, C., Tsanev, V. I., Delfosse, T., Williams-Jones, G., Horton, K., and Mather, T. A.: SO₂ depletion in tropospheric volcanic plumes, *Geophysical Research Letters*, 31,
 10 doi:10.1029/2004GL019990, 2004.
- Millard, G. A., Mather, T. A., Pyle, D. M., Rose, W. I., and Thornton, B.: Halogen emissions from a small volcanic eruption: Modeling the peak concentrations, dispersion, and volcanically induced ozone loss in the stratosphere, *Geophysical Research Letters*, 33, L24113, doi:10.1029/2006GL026959, 2006.
- Mori, T., Hashimoto, T., Terada, A., Yoshimoto, M., Kazahaya, R., Shinohara, H., and Tanaka, R.: Volcanic plume
 15 measurements using a UAV for the 2014 Mt. Ontake eruption, *Earth, Planets and Space*, 68, 1861, doi:10.1186/s40623-016-0418-0, 2016.
- Noguchi, K. and Kamiya, H.: Prediction of volcanic eruption by measuring the chemical composition and amounts of gases, *Bulletin of Volcanology*, 26, 367–378, doi:10.1007/BF02597298, 1963.
- O’Dowd, C. D., Jimenez, J. L., Bahreini, R., Flagan, R. C., Seinfeld, J. H., Hämeri, K., Pirjola, L., Kulmala, M., Jennings, S.,
 20 G., and Hoffmann, T.: Marine aerosol formation from biogenic iodine emissions, *Nature*, 417, 632, doi:10.1038/nature00775, 2002.
- Oppenheimer, C., Kyle, P., Eisele, F., Crawford, J., Huey, G., Tanner, D., Kim, S., Mauldin, L., Blake, D., Beyersdorf, A., Buhr, M., and Davis, D.: Atmospheric chemistry of an Antarctic volcanic plume, *Journal of Geophysical Research*, 115, 5473, doi:10.1029/2009JD011910, 2010.
- 25 Oppenheimer, C., Tsanev, V. I., Braban, C. F., Cox, R. A., Adams, J. W., Aiuppa, A., Bobrowski, N., Delmelle, P., Barclay, J., and McGonigle, A. J.S.: BrO formation in volcanic plumes, *Geochimica et Cosmochimica Acta*, 70, 2935–2941, doi:10.1016/j.gca.2006.04.001, 2006.
- Platt, U. and Bobrowski, N.: Quantification of volcanic reactive halogen emissions, in: *Volcanism and global environmental change*, Schmidt, A., Fristad, K., and Elkins-Tanton, L. T. (Eds.), Cambridge University Press, Cambridge, 115–132,
 30 2015.
- Platt, U. and Stutz, J.: Differential absorption spectroscopy, in: *Differential Optical Absorption Spectroscopy*, Springer, 135–174, 2008.
- Pyle, D. M. and Mather, T. A.: Halogens in igneous processes and their fluxes to the atmosphere and oceans from volcanic activity: A review, *Chemical Geology*, 263, 110–121, doi:10.1016/j.chemgeo.2008.11.013, 2009.



- Roberts, T.: Ozone Depletion in Tropospheric Volcanic Plumes: From Halogen-Poor to Halogen-Rich Emissions, *Geosciences*, 8, 68, doi:10.3390/geosciences8020068, 2018.
- Roberts, T. J., Braban, C. F., Martin, R. S., Oppenheimer, C., Adams, J. W., Cox, R. A., Jones, R. L., and Griffiths, P. T.:
 Modelling reactive halogen formation and ozone depletion in volcanic plumes, *Chemical Geology*, 263, 151–163,
 5 doi:10.1016/j.chemgeo.2008.11.012, 2009.
- Roberts, T. J., Martin, R. S., and Jourdain, L.: Reactive bromine chemistry in Mount Etna's volcanic plume: The influence of
 total Br, high-temperature processing, aerosol loading and plume–air mixing, *Atmospheric Chemistry and Physics*, 14,
 11201–11219, doi:10.5194/acp-14-11201-2014, 2014.
- Roberts, T. J., Vignelles, D., Liuzzo, M., Giudice, G., Aiuppa, A., Coltelli, M., Salerno, G., Chartier, M., Couté, B., Berthet,
 10 G., Lurton, T., Dulac, F., and Renard, J.-B.: The primary volcanic aerosol emission from Mt Etna: Size-resolved
 particles with SO₂ and role in plume reactive halogen chemistry, *Geochimica et Cosmochimica Acta*, 222, 74–93,
 doi:10.1016/j.gca.2017.09.040, 2018.
- Roberts, T., Dayma, G., and Oppenheimer, C.: Reaction Rates Control High-Temperature Chemistry of Volcanic Gases in
 Air, *Front. Earth Sci.*, 7, 1441, doi:10.3389/feart.2019.00154, 2019.
- 15 Rose, W. I., Millard, G. A., Mather, T. A., Hunton, D. E., Anderson, B., Oppenheimer, C., Thornton, B. F., Gerlach, T. M.,
 Viggiano, A. A., Kondo, Y., Miller, T. M., and Ballenthin, J. O.: Atmospheric chemistry of a 33–34 hour old volcanic
 cloud from Hekla Volcano (Iceland): Insights from direct sampling and the application of chemical box modeling,
Journal of Geophysical Research, 111, Q08008, doi:10.1029/2005JD006872, 2006.
- Rüdiger, J., Bobrowski, N., Liotta, M., and Hoffmann, T.: Development and application of a sampling method for the
 20 determination of reactive halogen species in volcanic gas emissions, *Analytical and bioanalytical chemistry*, 52, 325,
 doi:10.1007/s00216-017-0525-1, 2017.
- Rüdiger, J., Tirpitz, J.-L., Moor, J. M. de, Bobrowski, N., Gutmann, A., Liuzzo, M., Ibarra, M., and Hoffmann, T.:
 Implementation of electrochemical, optical and denuder-based sensors and sampling techniques on UAV for volcanic
 gas measurements: Examples from Masaya, Turrialba and Stromboli volcanoes, *Atmospheric Measurement Techniques*,
 25 11, 2441–2457, doi:10.5194/amt-11-2441-2018, 2018.
- Saiz-Lopez, A. and von Glasow, R.: Reactive halogen chemistry in the troposphere, *Chemical Society reviews*, 41, 6448–
 6472, doi:10.1039/c2cs35208g, 2012.
- Saiz-Lopez, A., Plane, J. M. C., Baker, A. R., Carpenter, L. J., Glasow, R. v., Martín, J. C. G., McFiggans, G., and Saunders,
 R. W.: Atmospheric chemistry of iodine, *Chemical reviews*, 112, 1773–1804, doi:10.1021/cr200029u, 2012.
- 30 Sander, R., Baumgaertner, A., Gromov, S., Harder, H., Jöckel, P., Kerkweg, A., Kubistin, D., Regelin, E., Riede, H., Sandu,
 A., Taraborrelli, D., Tost, H., and Xie, Z.-Q.: The atmospheric chemistry box model CAABA/MECCA-3.0,
Geoscientific Model Development, 4, 373–380, doi:10.5194/gmd-4-373-2011, 2011.



- Sander, R., Jöckel, P., Kirner, O., Kunert, A. T., Landgraf, J., and Pozzer, A.: The photolysis module JVAL-14, compatible with the MESSy standard, and the JVal PreProcessor (JVPP), *Geosci. Model Dev.*, 7, 2653–2662, doi:10.5194/gmd-7-2653-2014, 2014.
- Schönhardt, A., Richter, A., Theys, N., and Burrows, J. P.: Space-based observation of volcanic iodine monoxide, *Atmospheric Chemistry and Physics*, 17, 4857–4870, doi:10.5194/acp-17-4857-2017, 2017.
- Shinohara, H.: A new technique to estimate volcanic gas composition: Plume measurements with a portable multi-sensor system, *Journal of Volcanology and Geothermal Research*, 143, 319–333, doi:10.1016/j.jvolgeores.2004.12.004, 2005.
- Simpson, W. R., Glasow, R. von, Riedel, K., Anderson, P., Ariya, P., Bottenheim, J., Burrows, J., Carpenter, L. J., Frieß, U., Goodsite, M. E., Heard, D., Hutterli, M., Jacobi, H.-W., Kaleschke, L., Neff, B., Plane, J., Platt, U., Richter, A., Roscoe, H., Sander, R., Shepson, P., Sodeau, J., Steffen, A., Wagner, T., and Wolff, E.: Halogens and their role in polar boundary-layer ozone depletion, *Atmospheric Chemistry and Physics*, 7, 4375–4418, doi:10.5194/acp-7-4375-2007, 2007.
- Stix, J., de Moor, J. M. de, Rüdiger, J., Alan, A., Corrales, E., D’Arcy, F., Diaz, J. A., and Liotta, M.: Using Drones and Miniaturized Instrumentation to Study Degassing at Turrialba and Masaya Volcanoes, Central America, *Journal of Geophysical Research: Solid Earth*, doi:10.1029/2018JB015655, 2018.
- Surl, L., Donohoue, D., Aiuppa, A., Bobrowski, N., and Glasow, R. von: Quantification of the depletion of ozone in the plume of Mount Etna, *Atmospheric Chemistry and Physics*, 15, 2613–2628, doi:10.5194/acp-15-2613-2015, 2015.
- Symonds, R. B., Rose, W. I., Bluth, G. J. S., and Gerlach, T. M.: Volcanic-gas studies; methods, results, and applications, *Reviews in Mineralogy and Geochemistry*, 30, 1–66, 1994.
- Theys, N., Smedt, I. de, van Roozendaal, M., Froidevaux, L., Clarisse, L., and Hendrick, F.: First satellite detection of volcanic OCIO after the eruption of Puyehue-Cordón Caulle, *Geophysical Research Letters*, 41, 667–672, doi:10.1002/2013GL058416, 2014.
- Theys, N., van Roozendaal, M., Dils, B., Hendrick, F., Hao, N., and Mazière, M. de: First satellite detection of volcanic bromine monoxide emission after the Kasatochi eruption, *Geophysical Research Letters*, 36, doi:10.1029/2008GL036552, 2009.
- Vogel, L.: Volcanic plumes: Evaluation of spectroscopic measurements, early detection, and bromine chemistry, Heidelberg University Library, 2012.
- von Glasow, R.: Atmospheric chemistry in volcanic plumes, *Proceedings of the National Academy of Sciences of the United States of America*, 107, 6594–6599, doi:10.1073/pnas.0913164107, 2010.
- von Glasow, R., Bobrowski, N., and Kern, C.: The effects of volcanic eruptions on atmospheric chemistry, *Chemical Geology*, 263, 131–142, doi:10.1016/j.chemgeo.2008.08.020, 2009.
- Weber, K., Eliasson, J., Vogel, A., Fischer, C., Pohl, T., van Haren, G., Meier, M., Grobéty, B., and Dahmann, D.: Airborne in-situ investigations of the Eyjafjallajökull volcanic ash plume on Iceland and over north-western Germany with light aircrafts and optical particle counters, *Atmospheric Environment*, 48, 9–21, doi:10.1016/j.atmosenv.2011.10.030, 2012.



Wennberg, P.: Atmospheric chemistry: Bromine explosion, *Nature*, 397, 299–301, 1999.

Witt, M. L. I., Mather, T. A., Pyle, D. M., Aiuppa, A., Bagnato, E., and Tsanev, V. I.: Mercury and halogen emissions from Masaya and Telica volcanoes, Nicaragua, *Journal of Geophysical Research*, 113, doi:10.1029/2007JB005401, 2008.

5 Wittmer, J., Bobrowski, N., Liotta, M., Giuffrida, G., Calabrese, S., and Platt, U.: Active alkaline traps to determine acidic-gas ratios in volcanic plumes: Sampling techniques and analytical methods, *Geochemistry, Geophysics, Geosystems*, 15, 2797–2820, doi:10.1002/2013GC005133, 2014.